

Review

# Experimental/Numerical Investigation and Prediction of Fouling in Multiphase Flow Heat Exchangers: A Review

Rached Ben-Mansour <sup>1,2,\*</sup> , Sami El-Ferik <sup>3,4</sup> , Mustafa Al-Naser <sup>5</sup>, Bilal A. Qureshi <sup>1,2</sup>,  
Mohammed Ahmed Mohammed Eltoum <sup>4</sup> , Ahmed Abuelyamen <sup>1</sup>, Fouad Al-Sunni <sup>4</sup>   
and Ridha Ben Mansour <sup>2</sup> 

- <sup>1</sup> Mechanical Engineering Department, King Fahd University of Petroleum and Minerals, Dhahran 31261, Saudi Arabia  
<sup>2</sup> IRC for Renewable Energy and Power Systems, King Fahd University of Petroleum and Minerals, Dhahran 31261, Saudi Arabia  
<sup>3</sup> IRC for Smart Mobility and Logistics, Dhahran 31261, Saudi Arabia  
<sup>4</sup> Systems Engineering Department, King Fahd University of Petroleum and Minerals, Dhahran 31261, Saudi Arabia  
<sup>5</sup> Yokogawa Saudi Arabia, Dhahran 34464, Saudi Arabia  
\* Correspondence: rmansour@kfupm.edu.sa

**Abstract:** Fouling build-up is one of the most challenging problems for heat exchangers in industry. The presence of fouling leads to a degradation of system efficiency, an increase in operating cost, and possibly, a harmful environmental impact. For this reason, fouling analysis has become an extremely important research subject in order to have a safe and efficient operation. The analysis is more difficult where phase change of fluids is involved during the heat transfer process, as in the case of boilers and condensers, which are critical units in industrial facilities. Due to the lack of a comprehensive review of fouling analysis for the case of multiphase heat exchangers, this paper examines available approaches and techniques used for fouling characterization, modeling, monitoring, and prediction in heat exchangers for both single-phase and multiphase heat exchangers with a focus on fouling in thermal desalination systems. It also gives an overview of heat exchanger condition monitoring solutions available in the market.

**Keywords:** fouling characterization; phase change; modeling; monitoring; heat exchangers; desalination



**Citation:** Ben-Mansour, R.; El-Ferik, S.; Al-Naser, M.; Qureshi, B.A.; Eltoum, M.A.M.; Abuelyamen, A.; Al-Sunni, F.; Ben Mansour, R. Experimental/Numerical Investigation and Prediction of Fouling in Multiphase Flow Heat Exchangers: A Review. *Energies* **2023**, *16*, 2812. <https://doi.org/10.3390/en16062812>

Academic Editors: Sergio Nardini and Bernardo Buonomo

Received: 13 December 2022  
Revised: 24 January 2023  
Accepted: 13 March 2023  
Published: 17 March 2023



**Copyright:** © 2023 by the authors. Licensee MDPI, Basel, Switzerland. This article is an open access article distributed under the terms and conditions of the Creative Commons Attribution (CC BY) license (<https://creativecommons.org/licenses/by/4.0/>).

## 1. Introduction

The heat exchanger plays an essential role in a broad range of industrial applications where it facilitates heat transfer between two or more fluids. It enables heat transfer between two fluids that have different temperatures without direct contact. Heat is transferred by convection for each fluid and by conduction between fluids and the heat exchanger wall that separate them. Heat exchanger applications cover a broad range of industrial sectors, including petroleum industries, the petrochemical sector, sewage treatment, and thermal power plants.

A heat exchanger becomes fouled when undesirable materials build up on its inner surface, increasing thermal resistance and lowering thermal efficiency as a result [1]. The foulant, which can either be an organic or an inorganic material, usually has poor thermal conductivity compared to the metallic wall conductivity, which results in degradation of the heat transfer rate [2,3]. It also has an effect on the fluid cross-section, which increases the pressure drop and decreases the outlet temperature. Other negative consequences of fouling include blocked process tube bundles, corrosion, and pollution, see Figure 1 [4]. In general, such effects result in production losses and increased maintenance and cleaning costs. The cost linked to fouling in heat exchangers depends on its design, the nature of the fluids being handled, and the operating conditions [5,6].

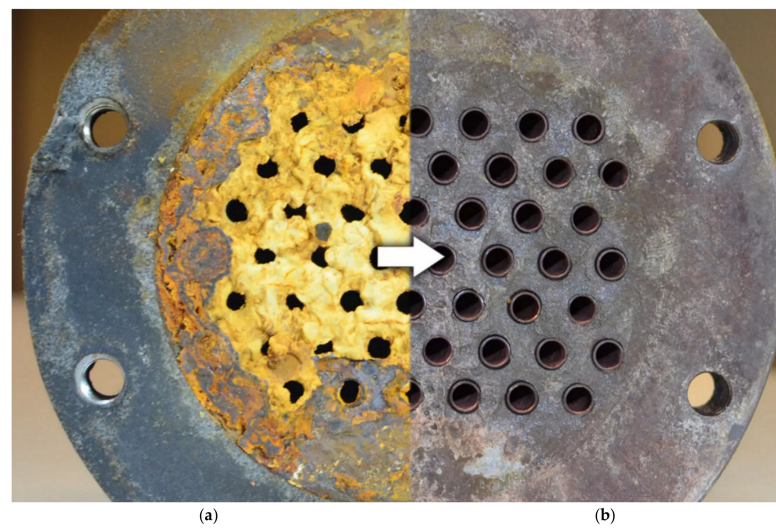


**Figure 1.** A bundle of heat exchanger tubes in (a) fouled state and (b) clean state [4].

Fouling occurs in two concurrent sub-processes: a deposit accumulation process and a removal process, as illustrated in Figure 2 [7]. Given the fouling formation mechanism, fouling can be grouped into the following six classes [8,9].

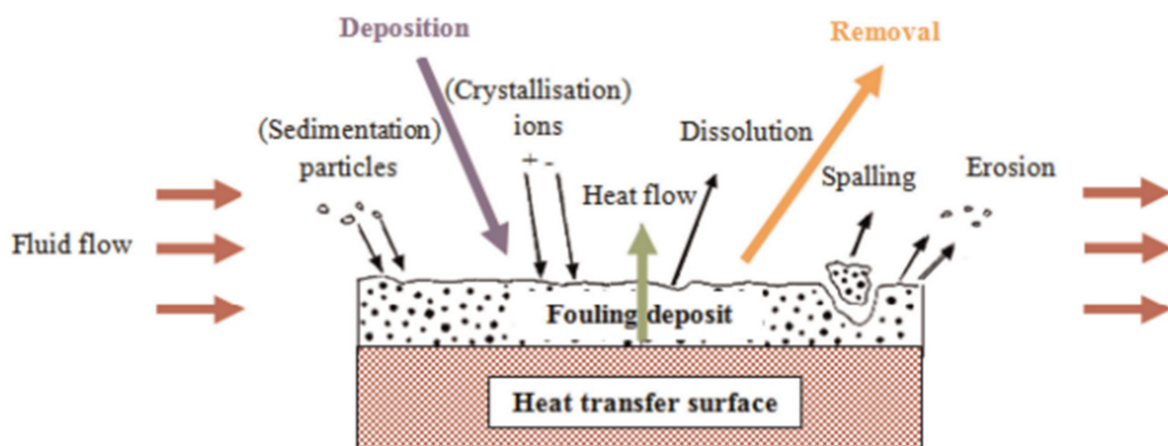


**Figure 2.** Overall fouling process [6].

- Scaling is a common fouling type often related to certain salts, such as calcium carbonate, naturally found in water. With an increase in temperature, these salts' solubility declines, which leads to the formation of deposits on the surface of the heat exchanger. It is hard to remove scale fouling using mechanical cleaning methods; therefore, the use of chemical methods may be inevitable. Figure 3 shows the accumulation of precipitated salts in the tubes of a heat exchanger [10].
- Particulate fouling is the formation of an insulating layer due to the accumulation of certain particles (such as sand) onto the heat exchanger surface.
- Corrosion fouling appears owing to a chemical reaction involving the heat exchanger material, which results in a corrosion product that reduces thermal conductivity.
- Chemical fouling results from a chemical reaction within the fluid streams, which leads to the formation of deposits on the heat transfer inner surface.
- Freezing fouling happens due to reducing the temperature of the hot stream close to the freezing point of one of its components.
- Biological fouling occurs due to the presence of biological organisms such as algae.



**Figure 3.** Accumulation of precipitated salts in heat exchanger tubes [4].

An increase in the fouling rates can lead to more equipment cleaning requirements. For mechanical cleaning, using high-pressure jetting requires opening the equipment and often bypassing the heat exchanger. The process must be shut down to allow access unless standby equipment has been provided. As a result, there is a time of lost production, which translates into a lower profit margin and a loss of return on the capital investment in the process equipment. Fouling is one of the many reasons for unscheduled shutdowns that result in lost productivity [10]. The cleaning costs range from USD 40,000 to USD 50,000 per heat exchanger per cleaning. The total cost of fouling in major industries is estimated to exceed USD 4.4 billion annually. The fouling of heat exchangers causes losses of about 0.25% to 30% of industrialized countries' gross domestic product (GDP) [11]. Additionally, heat exchangers and boilers account for 15% of a process plant's maintenance expenses, the majority of which can be attributed to fouling. According to recent studies, heat exchanger fouling may cause 1 to 2.5% of the world's CO<sub>2</sub> emissions and a 20% rise in the cost of fossil fuels [8,12].

Large pressure drops can increase the loads on the pumps, where the vaporization of the crude takes place within heat exchangers rather than the furnace, and reduce throughput. For a throughput-limited refinery processing 100,000 bbl/day, a 10% loss of production caused by a higher pressure drop would cost USD 20,000 per day, assuming USD 2/bbl for marginal lost production [13].

The economic cost of fouling can be summarized as [14]:

- Higher capital costs, additional heat transfer area, and cleaning equipment;
- Extra energy requirements to accommodate a lower energy recovery;
- Labor costs with additional maintenance;
- Cost of antifoulant chemicals;
- Reduced revenues;
- Equipment replacement costs.

The urgency to resolve this complicated issue has been aided by the significant expenses associated with fouling phenomena [15].

Heat exchanger efficiency is reduced in terms of heat transfer as a result of the increased thermal resistance. In general, the thermal conductivity of deposits is usually much lower than metals. As a result, even a thin layer of deposits can cause significant thermal resistance. Due to the increased turbulence produced by the roughness of elements, the fouling layer's surface, which is typically rougher than the original metal surface, may increase the heat transfer, which may counteract the effects of increased thermal resistance across the heat exchanger.

Fouling in refineries is considered to be the primary cause of energy loss in the chemical industry, accounting for up to 2% of total energy consumption [15]. The loss in refining

capacity caused by preheat train fouling was assessed to be 25,400 m<sup>3</sup>/day per year, and the refinery's overall fouling costs were estimated in 2003 to be USD 1.5 million over the course of three months [16]. An additional 31,800 m<sup>3</sup>/day capacity UK refinery reported in 2009 that a 1 °C reduction in preheat oil temperature costs the operator some GBP 250,000 annually [17].

The benefit to the refiners for reducing the fouling is increased capacity. Increasing on-stream time due to reduced fouling/cleaning can lead to more savings in refineries. For example, Macchietto et al. [18] claimed that in some Texas heavy crude refineries, the loss from reduced production could amount to USD 10/bbl. A one-day production loss on a refinery producing 200,000 barrels per day is estimated to cost between USD 0.4 M and USD 2 M. The increase in energy demand has led to the reduction of light and low-sulfur crude oil reservoirs. As a result, crude oil is becoming heavier and more complex, and fouling formation is becoming an imminent problem in the petroleum industry [19].

Figure 4 shows heat exchanger temperature distribution under the presence of fouling, where  $T_1$  and  $T_6$  denote the temperature of the hot and cold fluids, respectively [5].

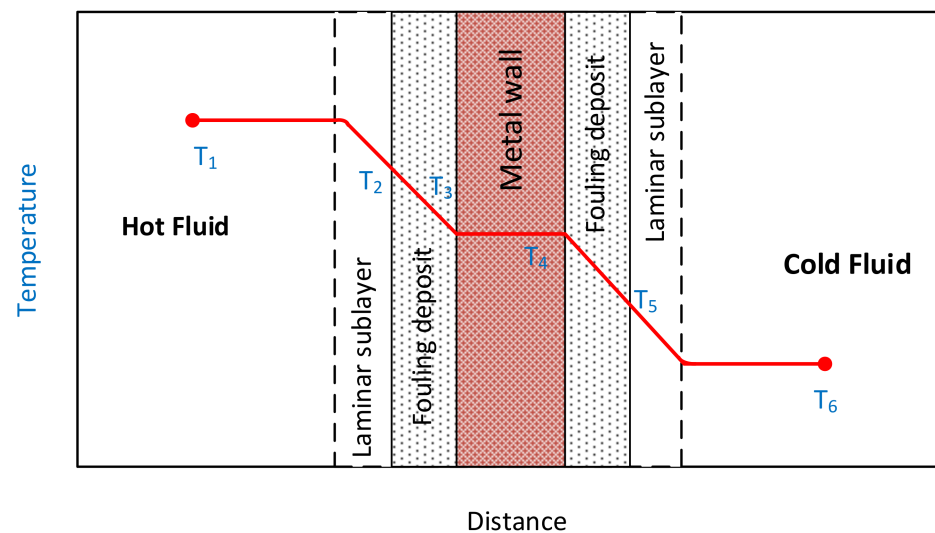


**Figure 4.** Temperature distribution of fouled heat exchanger (Adopted from [5]).

The heat transfer rate under steady-state conditions in a heat exchanger can be written as follows:

$$Q = UA\Delta T_{LMTD}F \quad (1)$$

where  $A$  is the area of heat transfer,  $U$  is the overall coefficient of heat transfer,  $\Delta T_{LMTD}$  is the logarithmic mean temperature difference given by Equation (2), and  $F$  is the correction factor for the  $LMTD$ .

$$\Delta T_{LMTD} = \frac{\Delta T_1 - \Delta T_2}{\log\left(\frac{\Delta T_1}{\Delta T_2}\right)} \quad (2)$$

where  $\Delta T_1$  and  $\Delta T_2$  represent the temperature difference between hot and cold fluids at the heat exchanger's inlet and outlet, respectively.

For the fouled heat exchanger, the overall heat transfer coefficient is given by

$$\frac{1}{U_f} = \left(\frac{x_1}{\lambda_1}\right) + \left(\frac{x_2}{\lambda_2}\right) + \frac{x_m}{\lambda_m} + \frac{1}{\alpha_1} + \frac{1}{\alpha_2} = R_T \quad (3)$$

where  $x_1$ ,  $x_2$ , and  $x_m$  represent the thickness of the deposit on the hot side, deposit on the cold side, and the metallic wall, respectively, while  $\lambda_1$ ,  $\lambda_2$ , and  $\lambda_m$  represent the thermal conductivity of deposit #1, deposit #2, and the metallic wall, respectively.  $\alpha_1$  is the convective heat transfer coefficient for the hot fluid while  $\alpha_2$  denotes the convective heat transfer coefficient for the cold fluid.  $R_T$  refers to the total thermal resistance per unit

area. Equation (3) illustrates the effect of fouling on the heat transfer coefficient, where the increase in deposits increases thermal resistance.

For the clean heat exchanger,  $U$  is given by

$$\frac{1}{U_C} = \frac{x_m}{\lambda_m} + \frac{1}{\alpha_1} + \frac{1}{\alpha_2} \quad (4)$$

This article is organized as follows. Section 2 presents the modeling of fouling in single and multi-phase flow systems. Section 3 explains the fouling modeling in thermal desalination systems. Section 4 sheds light on the major challenges related to multiphase flow fouling, while Section 5 concludes the paper.

## 2. Modeling of Fouling in Heat Exchange Systems

### 2.1. Single-Phase Flow Heat Exchangers

Although the object of this paper is fouling in multiphase heat exchangers, it would be useful to give an overview of fouling in single-phase systems. One of the early manuscripts that addressed the fouling problem was compiled by Melo, Bott, and Bernardo (1988) based on a NATO proceeding [20]. The manuscript, entitled *Fouling Science and Technology*, addressed topics on the physical nature of fouling, such as particulate fouling, adhesion, biological fouling, chemical reaction fouling, and crystallization fouling. Mathematical models were presented and supported by experimental data. The manuscript also presented research on the effect of fouling on the design and operation of heat exchangers, food processing, industrial water systems, and furnaces. Discussions on the economic impact of fouling, cleaning methods, and fouling monitoring were included. However, the manuscript did not address fouling in multiphase systems. Bott wrote a book on fouling in heat exchangers [5], where he addressed the same topics but in a more detailed and systematic manner. Many review papers have been written on fouling in general and fouling in heat exchangers in particular, but the majority do not address fouling in multiphase systems. A few review articles are discussed next to give an idea of where the focus on fouling modeling and research is heading.

Kuruneru et al. [21] looked at fouling in porous foam heat exchangers, which are considered to be the heat exchangers to be deployed in the future, as advised by the US Department of Energy. However, these heat exchangers are highly prone to fouling. The authors hope that gaining more understanding of the fouling mechanism in these types of heat exchanger surfaces using computational model techniques will pave the way to a desirable implementation of this technology in the near future. Heu et al. [22] discussed the development of anti-frosting and anti-fouling surfaces for outdoor heat exchangers widely used in air-conditioning systems and heat pumps. The authors reviewed the recent research work conducted on three types of surfaces, namely super-hydrophilic, super-hydrophobic, and slippery surfaces, in order to mitigate fouling. Along the same direction, Idumah et al. [23] looked at the recent development in nanotechnological advancement in polymer–nanocomposite coatings for antifouling purposes. They cited three anti-fouling methodologies, i.e., physical, chemical, and biological. The physical techniques entail modification of heat exchanger surfaces at the micro- and nano-level. The chemical techniques include self-polishing polymers and the release of anti-fouling coating agents. The biological methods include natural anti-fouling coatings as well as enzyme-oriented coatings.

Awais and Bhuiyan conducted a review [24] on the mitigation of fouling in heat exchangers. They focused on the impact of fouling on the transport phenomena in terms of flow and heat transfer. They discussed the effect of different parameters on the formation of fouling as well as its mitigation. These parameters include the mass flow rate, the inlet temperature variation, material surfaces, and other miscellaneous factors.

As far as monitoring goes, a recent review by Wen et al. [25] looked at the work done on a multi-resolution wavelet neural network approach for fouling resistance forecasting. They indicated that this method had outperformed the traditional neural network methods in forecasting the fouling in a plate heat exchanger.

Before we start our review on fouling in multiphase systems, it would be useful to present a simple and useful model that has been verified experimentally for fouling in single-phase systems. According to Kern and Seaton [26], the rate of change in deposition mass could be defined as follows:

$$\frac{dm}{dt} = \phi_D - \phi_R \quad (5)$$

where  $m$ ,  $\phi_D$ ,  $\phi_R$  represent deposited mass, deposition rate, and removal rate, respectively. In the case of asymptotic fouling, as depicted in Figure 5, fouling resistance per unit area ( $R_{fa}$ ) is given by:

$$R_{fa} = R_f^* \left(1 - e^{-t/\tau_c}\right) \quad (6)$$

where  $R_f^*$  is the fouling saturation (or asymptotic) value while  $\tau_c$ , called the time constant, is related to the properties of the system. It is the time when fouling resistance reaches 63.2% of its asymptotic value.

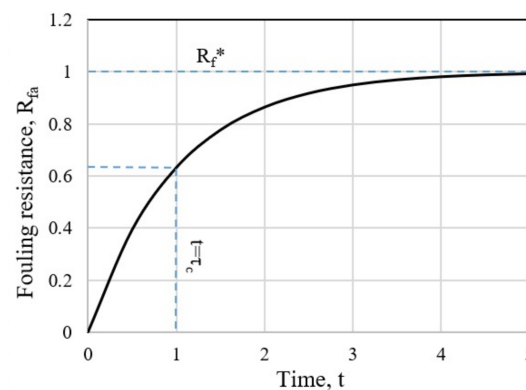


**Figure 5.** Asymptotic fouling.

## 2.2. Multiphase Flow Heat Exchangers

Liu et al. [27] conducted a CFD simulation for sub-cooled boiling flow in a channel with a length of 365.4 m under a uniform heat flux. The first two-thirds of the channel length is clean, while the rest is filled by a layer of fouling with thickness varying from 0 to 1.55 mm. In addition to the effect of fouling thickness on heat transfer and pressure reduction, the impact of initial velocity was also investigated in their study. They fixed the thermal conductivity of the fouling layer to be  $0.173 \text{ W/m}^2 \cdot \text{K}$ . Figure 3 shows that the onset of steam occurs at a distance of 0.5 m from the entrance, where the volume fraction is between 0.45 and 0.6 until it reaches the location of the fouling layer. Then it jumps and varies according to the fouling layer thickness, where a higher vapor void fraction corresponds to a larger fouling thickness (Figure 6).

The heat transfer decreases with the presence of the fouling layer, and it decreases considerably with the increase in the fouling thickness compared to that without the fouling layer (Figure 7). Nevertheless, the effect of heat transfer in the region free of fouling shows a similar trend. The average number of Nusselt in the region of fouling with a deposited layer of fouling drops approximately 50 times more than without fouling.

Figure 8 indicates that, in the fouling region, the heat transfer performance with a thickness of 0.225 mm is 5 times the one with a thickness of 1.55 mm. Increasing the fouling layer thickness results in a higher bulk temperature of the heating wall in the area that is exposed to fouling. This temperature should not exceed a certain value due to safety issues (700 K for the system in a nuclear station). According to the variation in the heating wall temperature with fouling thickness, there is an increase of about 130 K for each 1 mm of fouling thickness. Hence, the fouling thickness can be estimated from the bulk temperature, which can be very useful for developing and implementing an economic plan for cleaning

the fouling layer. Their geometry has a nine-fin extension distributed along the channel; therefore, the total pressure has a staircase-like profile (See Figure 9). They stated that the total pressure does not decrease as the thickness of the fouling layer increases along the channel.

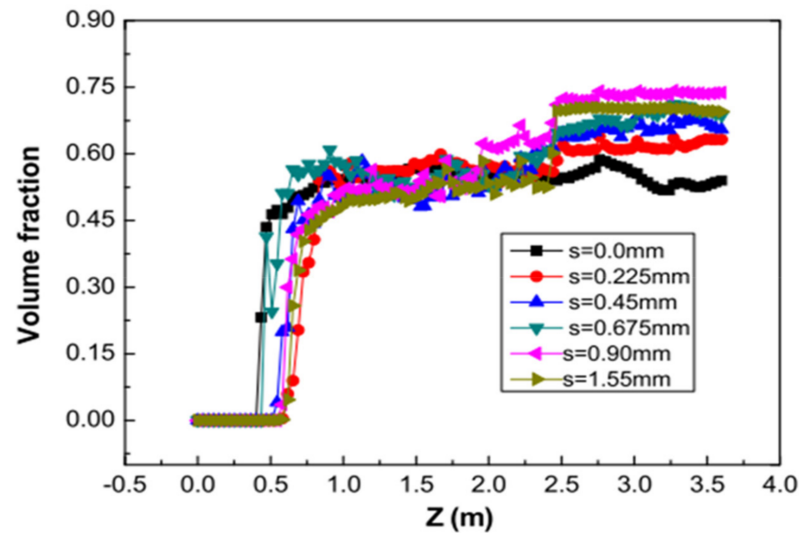


Figure 6. Volume fraction along a tube for varying fouling layer thickness [27].

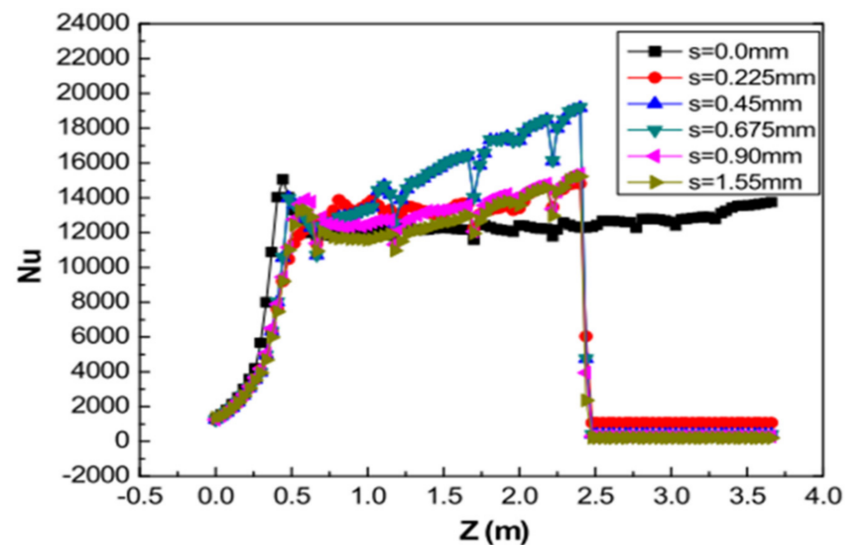
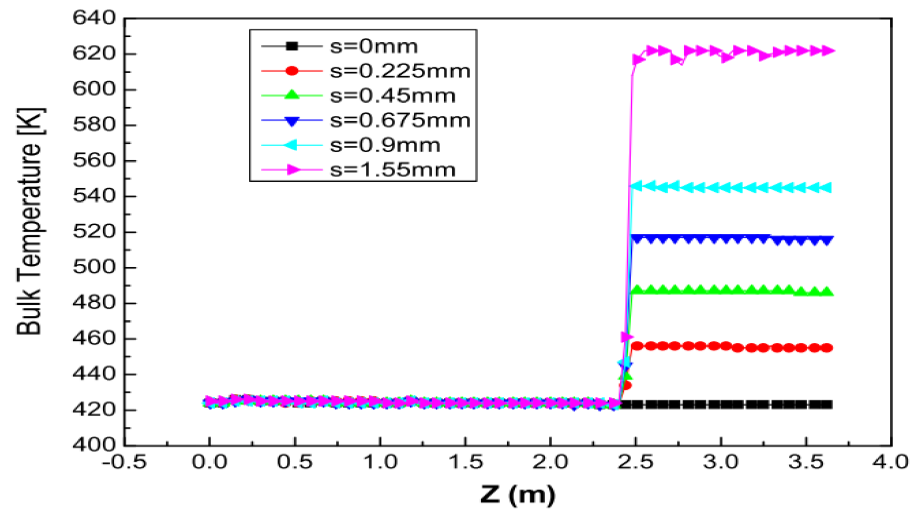
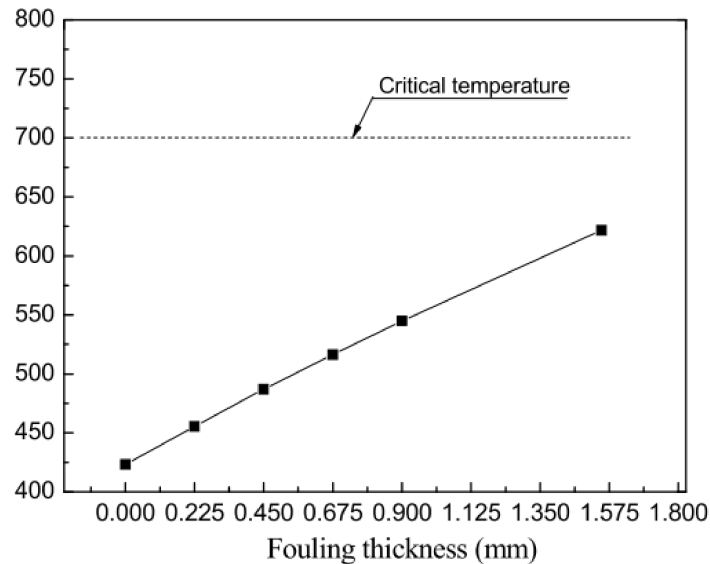


Figure 7. Nusselt number along a tube for varying fouling layer thickness [27].

The effect of the initial velocity was conducted for a fouling thickness of 1.55 mm, and the analysis was carried out by magnifying the velocity up to six times (see Figure 10). It affected the bulk temperature near the inlet area and near the fins area in the region of fouling only. The pressure drops occurred due to increasing velocity, while the fouling region did not show a clear effect on pressure drop. However, the vapor volume fraction was affected by the value of the initial velocity, where the onset of the boiling was delayed with its increase. Moreover, the vapor void fraction jumps to a higher value as the flow enters the fouling region in each case of the initial velocity.



(a) along the channel



(b) in the fouling region

**Figure 8.** Bulk temperature along a tube for varying fouling layer thickness [27].

Helalizadeh et al. [28] investigated experimentally scale formation from solutions of mixed inorganic salts and showed the presence of co-precipitation of two dissolved inorganic salts ( $\text{CaSO}_4$  and  $\text{CaCO}_3$ ) in the scale. They studied the effect of operational parameters (fluid velocity, heat flux, surface/bulk temperatures, and concentration of the solutions) on fouling resistance during convective heat transfer and sub-cooled flow boiling. Scale formation during the sub-cooled flow boiling occurs as a result of a combination of two mechanisms. Firstly, fouling due to the mechanisms of bubble formation and microlayer of evaporation (i.e., in the area affected by bubble formation). Secondly, the fouling that takes place due to the convection mechanism. A linear increase in fouling resistance over time is indicated by the majority of measured fouling curves. Hard and adherent deposits are typically characterized by a linear relationship, which means that either the deposition rate is constant and there is no removal or the difference between the deposition rate and removal rate is constant.

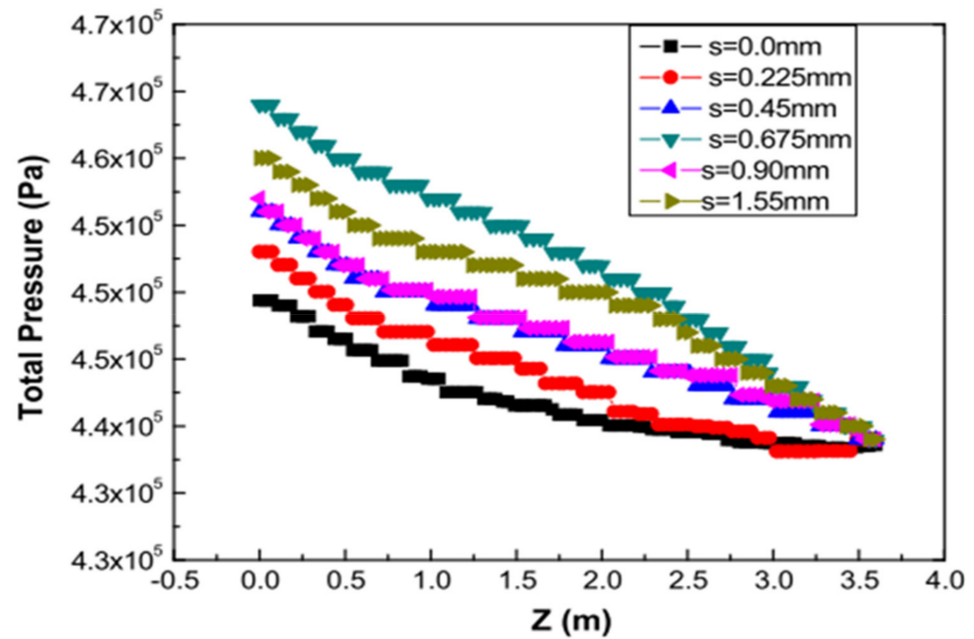


Figure 9. Variation of the pressure along the tube [27].

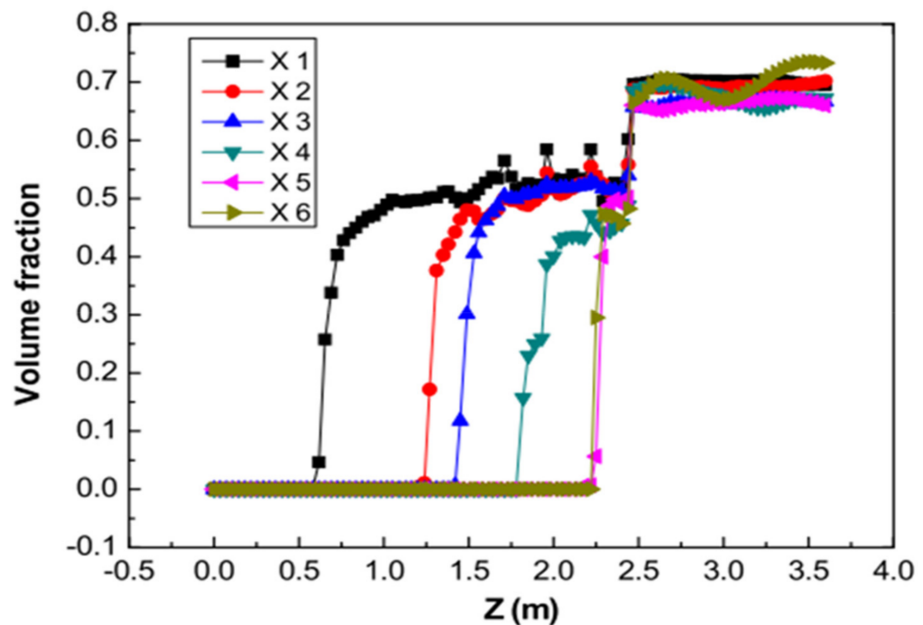


Figure 10. Volume fraction along the tube at various velocities [27].

The effect of fluid velocity on fouling resistance was reflected by varying velocity from 40 to 100 cm/s (Figure 11). In all cases, the fouling curves show an approximately linear increase in fouling with time after an initial period of fast deposition. At lower velocities, the mass transfer boundary layer is relatively thick, and as a result, molecular diffusion has some influence on the fouling rate. Accordingly, the fouling process is governed by diffusion. In contrast, the boundary layer thickness is decreased at higher velocity values. Thus, mass transfer across the boundary layer is no longer affected by the fouling rate, indicating that the fouling is controlled by a chemical reaction.

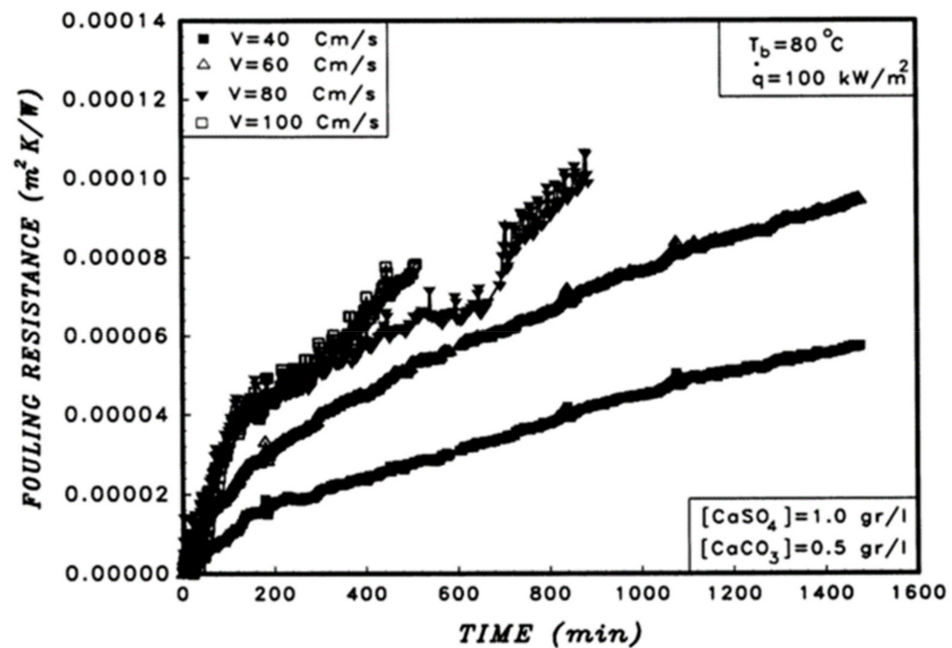


Figure 11. Variation of fouling resistance with time at different velocities [28].

Furthermore, according to their results, different trends of fouling resistance were observed for different surface temperatures (Figure 12) where different regimes can exist, such as forced convective heat transfer ( $T_s = 103\text{ }^\circ\text{C}$ ) and sub-cooled flow boiling ( $T_s = 107\text{ }^\circ\text{C}$  and  $113\text{ }^\circ\text{C}$ ). It can be seen from Figure 13 that during the initial period (time < 500 s), fouling resistance for subcooled flow boiling regimes is smaller than in the case of force convective regimes. However, after some time, it exceeds the resistance of force convective flow, where higher heat flux would generate more fouling resistance. Moreover, the rate of fouling shows slight dependence on bulk temperature, which is indicative of the fact that fully-developed boiling did not achieve for the experimental conditions [28]. Additionally, they indicated that the degree of supersaturation of the deposit-forming species has more influence on crystallization fouling than the molar concentration.

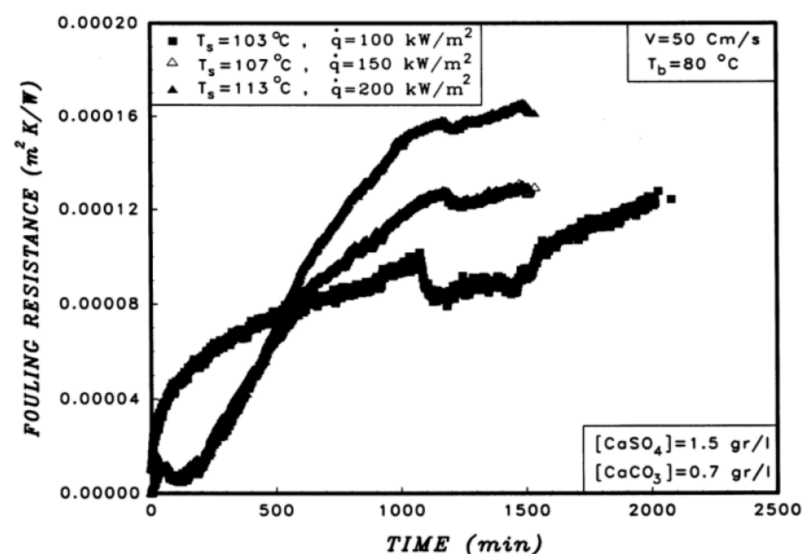


Figure 12. Variation of fouling resistance with time at different surface temperatures [28].

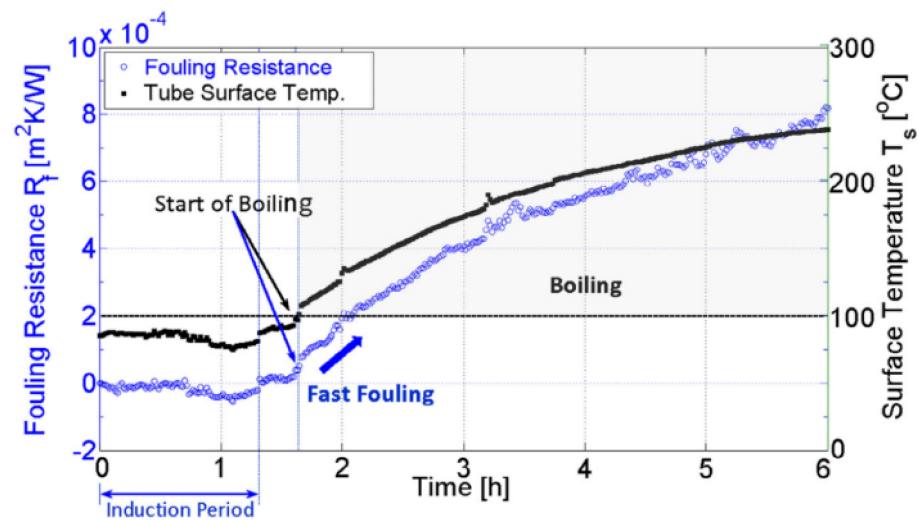


Figure 13. Change of fouling resistance during single-phase and two-phase [3].

Haghshenasfard et al. investigated the operational conditions of sub-cooled flow boiling as well as wall roughness [29]. They confirmed similar results as in the work of Helalizadeh and Mu [28] where the fouling resistance increased proportionally with the velocity and the fouling rate was slightly influenced by the bulk temperature while it increased as the surface temperature increased.

The crystallization process goes through three stages. The first phase is super-saturation, then the nucleation of crystals, and the last phase is the growth of crystals. In theory, crystallization fouling happens each time operational factors lead to the creation of super-saturation with regard to sparingly soluble salts such as  $\text{CaSO}_4$  or  $\text{CaCO}_3$ . The solubility properties of these salts exhibit an inverse trend. Thus, the principal factor that leads to fouling is local super-saturation [30,31]. Particularly, fouling during sub-cooled flow boiling is one of the most significant types of precipitation fouling, which happens in many process industries. The fouling formation by sub-cooled flow boiling and forced convective heat transfer differ in some ways [32]; firstly, the fouling resistance under the sub-cooled flow boiling conditions is substantially higher than in the case of convection heat transfer. Nevertheless, in the experiment of Helalizadeh and Mu [28], a reversed trend was shown but only during the initial period of time. Secondly, the interaction between the fouling and bubble nucleation led to severe corrosion of the heated surfaces. Thirdly, according to the mechanisms of bubble formation, the local concentration of calcium sulfate near the surface is noticeably higher than forced convection values. During the bubble formation through the surface, micro-layer evaporation results in localized calcium sulfate supersaturation at the gas–liquid–solid interface, which enhances deposit formation. It is typical for desalination units, steam boilers, and evaporators to experience scaling under flow boiling.

Some rough surfaces were studied for their susceptibility to fouling by Esawy [33]. He found that rough and porous surfaces demonstrated that they suffered much less fouling than smooth surfaces. Scale formation was enhanced by the creation of more nucleation sites due to added bubbles produced from the smooth surfaces. On the other hand, when a surface has a rough texture, it leads to an increase in bubble detachment velocity and results in the formation of a few scattered crystals.

Regarding the heat transfer model in multiphase flow, they can be categorized into seven types [34].

1. Enhanced model: For enhancement-factor type models, the flow boiling heat transfer coefficient  $h_{tp}$  may be reduced to ( $h_{tp} = \psi h_{sp}$ ). Where the term  $\psi$  denotes the enhancement factor and the subscript  $sp$  denotes single phase.

2. Nucleate boiling models: Considering nucleate boiling to be the main mechanism while ignoring the influence of other mechanisms.
3. Superposition models: It uses the superposition principle. In which the two-phase flow boiling process was mainly governed by the nucleate boiling mechanism and the forced convection mechanism, and the contributions made by the two mechanisms were additive. The first superposition model was formulated by Chen [35], where he assumed saturated nucleation flow boiling in addition to convective heat transfer combined to give the total heat transfer in multiphase flow ( $h_{tp} = S \cdot h_{nb} + F \cdot h_{sp,l}$ ). He developed graphical functions for  $S$  and  $F$ , which are difficult to be determined.
4. Asymptotic models: The contributions of the nucleate boiling and convective boiling components are taken into consideration in correlations for flow boiling heat transfer coefficients as follows: ( $h_{tp} = [(S \cdot h_{nb})^n + (F \cdot h_{sp,l})^n]^{1/n}$ ).
5. Largest mechanism predominant models: This type of modeling calculates the flow boiling heat transfer coefficients for each mechanism at first and then takes the largest value among the calculated coefficients as the result.
6. Flow pattern-based models: These are based on flow patterns and, therefore, provide some information about those flow patterns.
7. Hybrid models: The segmentation of flow regions utilizes a parameter as a criterion, followed by employing various methods to predict each distinct region, none of which belong to the above six models. For instance, using a combination of an asymptotic correlation and flow pattern-based method, Yoon et al. [36] categorized flow areas into two portions based on the critical quality criteria.

Fang et al. [34] reported that the correlation of their work in reference [37] was the most accurate at predicting each of the 19 fluids, including water. Moreover, they suggested the top five models that have high prediction accuracy for the entire database.

Esawy et al. [38] experimentally investigated the mechanism of crystallization fouling of finned tubes during nucleate pool boiling of  $\text{CaSO}_4$  solutions for different heat fluxes. The results show a higher dependence of fouling resistance, as a function of time, on the heat flux values. They divided the fouling curve into three regions (Figure 10); the first region is where there is a sharp increase in the fouling resistance due to the initial formation of deposits on the smooth tube. However, they indicated that this initial fouling layer would lead to a temporary increase in the number of bubble nucleation sites. Accordingly, an enhancement in the heat transfer would occur, which appears as a reduction in the fouling resistance in the second region. A similar trend was also observed in other studies [39]. The third region is where the fouling resistance starts to grow gradually due to the buildup of the fouling layers. Furthermore, it can be noticed from their results that the elapsed time for the first and second regions becomes smaller as the heat flux increases. Moreover, the finned tubes show high performance compared to the smooth tubes, especially at low heat fluxes where the fouling resistance fluctuates around zero. There is a subsequent bubble formation in the finned tubes, which creates a tremendous amount of turbulence during the bubble departure resulting in washing the frail deposit layer from the base surface. Additionally, the fouling curve in the finned tube reaches an asymptotic value after a short operating time.

Fukada et al. [40] conducted an experimental study to test the effect of fouling on nucleation pool boiling for small wires with and without fouling. They observed more vigorous bubbling on the fouled wire compared to that of the clean wire at the same heat flux. They mentioned that the enhancement of the bubbling is due to hydrophilic porous structures in the fouling which provides a sufficient number of active sites for bubbling nucleation. Nevertheless, the boiling curves for both wires are almost the same.

Crystallization fouling, which occurs during boiling heat transfer, is known to be superior to that in convective heat transfer. Thus, it is usually avoided by keeping the surface temperature below the boiling point. However, an experimental investigation by Abd-elhady MS and Malayeri [3] showed that a convective heat transfer flow exposed to a constant heat flux could be turned into sub-cooled boiling heat transfer after some time of

operation due to crystallization fouling which added more thermal resistance. Figure 13 shows the fouling resistance for a solution of water with  $\text{CaSO}_4$  of 4 g/L concentration. The solution enters a tube at  $40^\circ\text{C}$  while the tube is exposed to a constant heat flux, and its initial temperature is  $80^\circ\text{C}$ , which is much lower than the boiling temperature of the solution ( $105^\circ\text{C}$ ). At the early period of operation, a single-phase heat transfer is occurring, however, after some time, fouling layers start to build up, and it adds thermal resistance, which results in an increase in the surface temperature to values above the boiling temperature. Once the boiling heat transfer starts, the fouling resistance starts to increase dramatically. It should be emphasized that, in the boiling process, high scale concentration is formed after the bubbles leave the heated surface [3,32,39,41].

Wang et al. [42] tested the effect of heat flux and initial temperature on the characteristics of nanoparticles of  $\gamma\text{-Al}_2\text{O}_3$ /water under single-phase flow and sub-cooled flow boiling conditions. Figure 14 depicts the trends of in  $\gamma\text{-Al}_2\text{O}_3$  particulate fouling resistance curve under different heat fluxes. In the single phase, the asymptotic value of fouling resistance drops as the heat flux increases until it reaches a minimum value, after which a further increase in heat flux leads to two-phase boiling heat transfer. While in the two-phase boiling heat transfer, any increase in the heat flux results in more fouling resistance. On the other hand, they reported that the inlet temperature had a negligible impact on the fouling resistance in the case of sub-cooled boiling, while it had a reverse relation with the fouling resistance in the case of single-phase heat transfer.

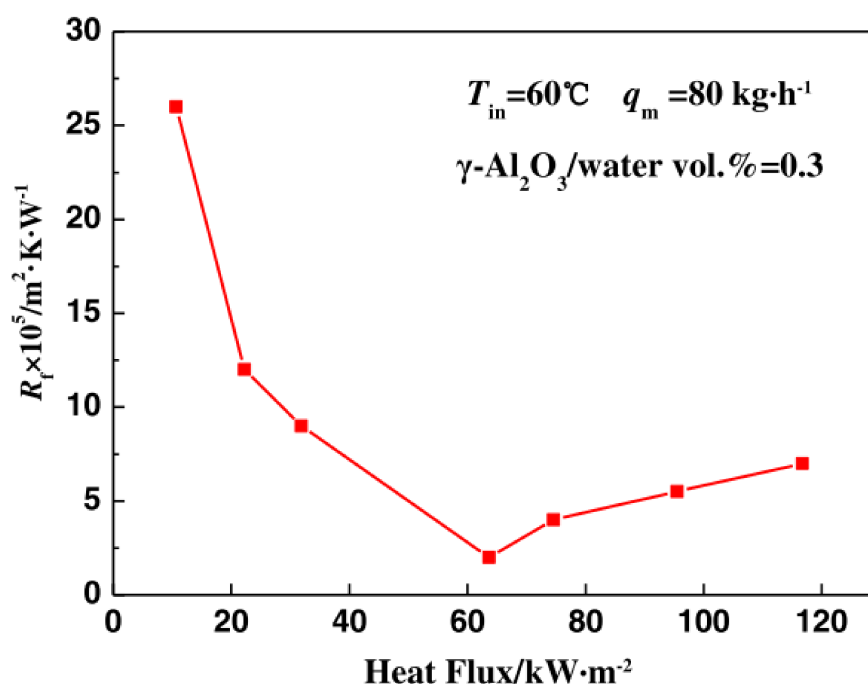


**Figure 14.** The asymptotic values of fouling resistance of  $\gamma\text{-Al}_2\text{O}_3$ /water vol.% = 0.3 under different heat fluxes [42].

We close this section with an important type of fouling that occurs in power utility boilers and furnaces which is ash fouling superheaters in steam boilers. This type occurs mainly for steam boilers fueled with coal which are still in operation in the USA, Europe, and China. Soot formation and slag can also occur in steam boilers operated with diesel and other heavy fuels. Many works have been published on this topic. Important works to be cited here include the works by Taler et al. [43]. In this work, the authors have developed a computational model for the tube heat exchangers in the superheater region of the steam boiler. They have included the ash fouling layer that gets deposited on the tubes. In the superheater region, the radiate transfer can amount to up to 90% of the total heat transfer,

and the determination of the radiative properties of the ash layer is very critical in obtaining a good prediction of the heat transfer and the production of the steam boiler.

### 3. Focus Area: Modeling of Fouling in Thermal Desalination Systems

#### 3.1. Fouling in Thermal Desalination Systems: Overview

Desalination is becoming more and more popular as an alternate source of water supply resources as many governments and utilities deal with pressures from population expansion, a lack of water resources, and stricter water quality requirements. Considering that there are more than 19,000 desalination facilities in the world, with a total production capacity of 100 million cubic per day of desalinated fresh water [44]. Presently, over 50% of installed desalination plants are located in the Middle East and North Africa region (MENA). Despite the new trend of increasing use of reverse osmosis desalination (SWRO) in this region, thermal desalination processes, mainly MSF, MED, and TVC-MED, are still the dominant technologies for producing drinking water. Fouling in desalination is an important consideration in the design and cost-effective operation of both thermal and membrane-based desalination technologies. For example, the scaling tendency in an MSF plant requires about 20 to 25% excess design allowance, which represents 6% of the total cost of MSF plants [45].

Thermal desalination is a phase change process based on the principles of evaporation and condensation. Thermal desalination includes two major technologies: Multi-Effect Distillation (MED) and Multi-Stage Flashing (MSF). In MED, the feed water is sprayed and distributed over the outside of the horizontal evaporator tubes for different effects making a falling thin film evaporation on the tube surfaces. Thus, the salinity rises, especially in the bottom tube row of the evaporator, to reach as much as 70 g/kg [46]. A potential scale can be formed outside the tube. On the other hand, in the MSF process, feed water moves through a sequence of vacuumed stages, and brine flows through the tubes and is preheated. The scale is formed inside the condenser tubes of the heat rejection (HRJ), heat recovery section (HRS), and the brine heater (BH). The typical trend of temperature and concentration gradients in different sections of an MSF distiller is shown in Figure 15 [47].

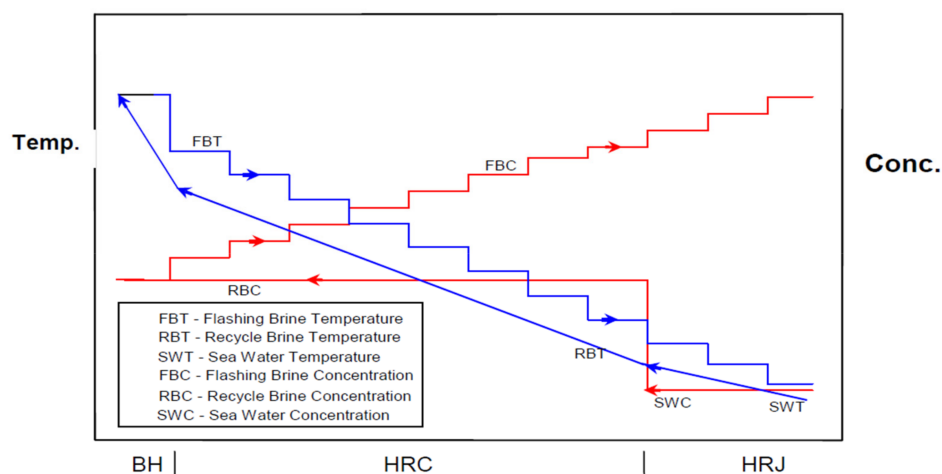
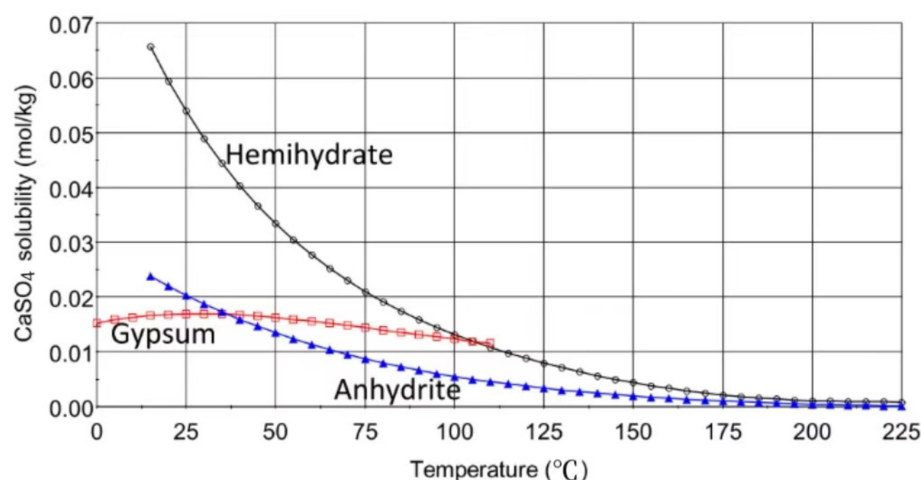


Figure 15. Temperature and concentration gradients in MSF distillers [47].

Fouling in thermal desalination is a process in which undesirable layers of inorganic seawater components are deposited inside (MSF plant) or outside (MED plant) of heat exchanger surfaces. With time, these materials continuously build up a fouling film causing an additional barrier to the heat transfer, increasing pressure drop, and possibly promoting corrosion of tube material. Consequently, these effects can increase specific energy consumption and create additional operating and maintenance costs [48–50].

Typically, seawater and brackish water contain high amounts of total dissolved ions and biological matter. The main scale-forming constituents of seawater and brackish

water are sparingly soluble ions such as calcium, magnesium, bicarbonate, sulfate, silica, etc. Under evaporation conditions, these sparingly soluble ions are concentrated and exceed their solubility limits leading to scale precipitation in distillers [46,51–56]. The scale precipitation in thermal desalination plants is mainly caused by the crystallization of two inorganic salts, calcium carbonate ( $\text{CaCO}_3$ ) and magnesium hydroxide  $\text{Mg}(\text{OH})_2$ , generally referred to as alkaline scales. The three forms of calcium sulfate ( $\text{CaSO}_4$ ), namely gypsum, anhydrite, and hemihydrate, can be crystallized at high concentration factors of saline water (1.8–2.0) and high temperature, usually above  $120\text{ }^\circ\text{C}$  [57–61]. The development of calcium sulfate salts, which is normally termed as “hard scale”, inside MED or MSF distillers should be mitigated by operating the plant at temperatures and/or brine concentrations lower than the solubility limits, as shown in Figure 16 [46].



**Figure 16.** The solubility of  $\text{CaSO}_4$  in its three different forms [47].

It is worth noting that calcium carbonate, magnesium hydroxide, and calcium sulfate are inverse solubility salts; their solubility in water decreases with temperature and salinity. Hence, MED and MSF operation is limited to top brine temperature and maximum brine salinity. In addition to mineral scales, particulate fouling, caused by a fine suspended matter, can occur, especially when the seabed is disturbed and suspended solid content increases as a result of various reactions, aggregation, and flocculation.

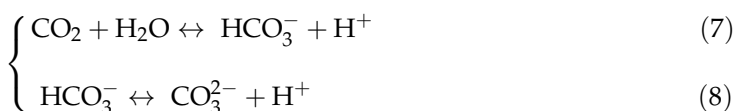
### 3.2. Thermodynamics and Kinetics of Inorganic Scales

Scale formation in thermal desalination comprises complex phenomena involving both fouling crystallization and transport mechanisms that take place simultaneously, such as surface and bulk diffusion of solute, partial and total dissolution of ions, and surface integration of ions [3,41]. Furthermore, scale formation is influenced by various solution compositions and operating conditions such as salt concentration, the diffusion rate of ions, operating temperature, flow velocity, pH of the water environment, and time as well as the release rate of  $\text{CO}_2$  [49,53,59,61,62]. The flux of carbon dioxide across the air–brine interface is derived from the difference in the partial pressure of  $\text{CO}_2$  in the atmosphere and in the surface seawater. Initially, the carbonate system ( $\text{HCO}_3^-$ ,  $\text{CO}_3^{2-}$ ,  $\text{CO}_2$ ,  $\text{H}^+$ , and  $\text{OH}^-$ ) present in seawater is in phase equilibrium. Any variation occurring in the system, i.e., in partial pressure of  $\text{CO}_2$  gas, results in a transformation of reacting systems from gas to liquid phase until chemical equilibrium between gas and solution phases is re-established. The carbonate ions concentration in the MSF and MED distillers controls the rate of precipitation and dissolution of the salt scale. A better knowledge of the thermodynamics of carbonate systems is essential for understanding the thermodynamics and kinetics of scale processes and the prediction of scale formation [63,64].

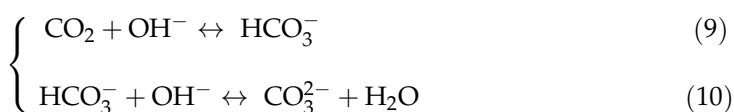
### 3.2.1. Equilibrium Modeling of Carbonate System in High Salinity Water

During the evaporation process in thermal desalination plants, the concentration of CO<sub>2</sub> increases and exceeds the saturation level, and CO<sub>2</sub> is released in the condensate. The liberation of CO<sub>2</sub> impairs the equilibria between HCO<sub>3</sub><sup>-</sup>, CO<sub>3</sub><sup>2-</sup>, CO<sub>2</sub>, H<sup>+</sup>, and OH<sup>-</sup> in the brine. A detailed investigation into the reaction of the carbonate system shows that the hydration and dehydration of CO<sub>2</sub> in the bicarbonate system follow the below acidic and alkaline reactions.

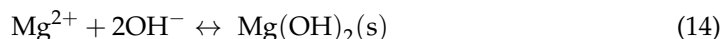
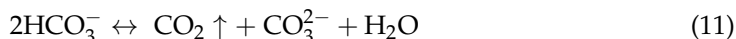
Acidic mechanism:



Alkaline mechanism:



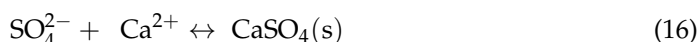
It is widely recognized that the thermal decomposition of the bicarbonate ions is responsible for the scale formation in thermal desalination plants. Nevertheless, there is still quite a controversy about the underlying kinetics of the precipitation of calcium carbonate or magnesium hydroxide [59,65–67]. Langelier et al. [66] proposed that calcium carbonate crystallization starts with the thermal decomposition of bicarbonate ions, resulting from precedent reactions (Equations (1)–(4)) to form carbonate ions (see Equation (11)), which in turn reacts with residual calcium to form the precipitation of calcium carbonate (see Equation (12)). In a strong alkaline solution, which is the case of the pH range in MED or MSF distillers, the alkaline mechanism predominates, particularly at high temperatures [48,52,61,68]. In this case, the hydrolysis of carbonate ions generates CO<sub>2</sub> and hydroxide ions (see Equation (13)), initiating magnesium hydroxide precipitation (see Equation (14)).



On the other hand, Dooly and Glater [65] suggested that the formation of magnesium hydroxide scale can occur simultaneously with the initial release of hydroxide ions (Equations (14) and (15)). Excess hydroxide ions are neutralized by bicarbonate ions to form carbonate ions, following the alkaline mechanism (Equation (10)), which combine with calcium leading to calcium carbonate crystallization (Equation (12)).



In the presence of sulfate ions, calcium ions can cause calcium sulfate scale once its solubility exceeds the supersaturated conditions:



The bulk composition of the supersaturated solution (SO<sub>4</sub><sup>2-</sup>, Ca<sup>2+</sup>, Mg<sup>2+</sup>, CO<sub>3</sub><sup>2-</sup>, HCO<sub>3</sub><sup>-</sup>, OH<sup>-</sup>) is transported towards the distiller surface due to the transport process and reacts at the heat transfer surface, leading to the formation of inorganic scale (CaCO<sub>3</sub>(s), Mg(OH)<sub>2</sub>, CaSO<sub>4</sub>(s)).

### 3.2.2. Models for Release of Carbon Dioxide in Seawater

Much research has focused on the development of models for CO<sub>2</sub> release and the carbonate system in thermal desalination distillers. The first investigations [69–71] are based on simple chemical reaction models and some experimental data. Mass transfer of ions to the brine surface was totally ignored. CO<sub>2</sub> release and alkaline scale formation were investigated experimentally in MSF distillers by extraction and chemically analyzing saline samples from water boxes and flash chambers [71]. Based on their analyses, the thermal decomposition of HCO<sub>3</sub><sup>−</sup> leading to the production of CO<sub>3</sub><sup>2−</sup> and OH<sup>−</sup> ions in excess depending on the operating temperature, heating time, and extent of aeration was demonstrated. In the work of Hasson and Perl [70], the mechanism of CaCO<sub>3</sub> scale deposition from a laminar falling film was fundamentally analyzed. A simplified physical model, based on the mass transfer process between the fluid and heated surface to calculate the CO<sub>2</sub> release, was developed. Hamrouni and Dhabi [56] developed a thermodynamic model of saline water that accounts for acid–base, ion association, and precipitation equilibrium using Extended Debye–Hückel and Pitzer models for the ion activity coefficient calculations. Additionally, they proposed calco–carbonic equilibrium curves for different kinds of saline water to predict the calcium carbonates and calcium sulfates stability. Rigorous electrolyte thermodynamics were applied to the modeling of MSF distillers, and scale formation along with CO<sub>2</sub> release was predicted by considering the equilibrium conditions of multi-component electrolyte solution [72].

The above-mentioned investigations did not combine the mass transfer and chemical reaction and the reaction kinetics involved in the CO<sub>2</sub> release process as well as in the precipitation process of mineral scales [64,73]. Consequently, a detailed investigation into the reaction kinetics of the carbonate system was proposed [47,60,62,74]. Moreover, the reaction mechanisms and kinetics of calcium carbonate scale deposit formation in thermal desalination processes were also studied. Consequently, a detailed model allowing the calculation of the ion concentration in the carbonate system of the brine was elaborated by Al-Rawajfeh et al. [73,75,76]. Based on their model, simulation results were experimentally verified by measuring the flow rates, temperature, pressure, and CO<sub>2</sub> concentrations continuously in the parallel vent of the two MSF distillers with a set of different operating conditions [73].

### 3.2.3. Kinetics of Inorganic Scale Deposit Formation

The salt crystallization in thermal desalination processes involves heat/mass transfer, chemical reaction equations, and phase equilibrium at the brine evaporator interface. It is often described with five mechanisms, as shown in Figure 17 [30].

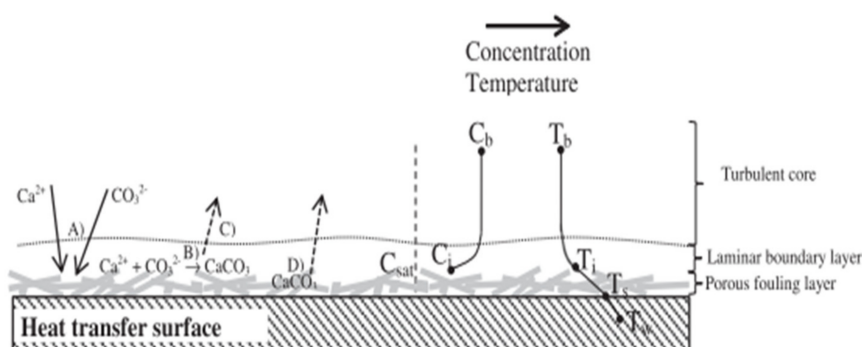


**Figure 17.** Illustration of the crystallization fouling mechanisms and the concentration and temperature profiles in the system.

- Initiation of scale by chemical reaction of the dissolved gas and nucleation of the fouling species at the heated surface.
- Transport of reacting bicarbonate systems from the bulk to the liquid interface by diffusion process ((A) in Figure 17) followed by

- Attachment of the scale deposition to the heated surface ((C) in Figure 17).
- Removal of crystals from fouling layer, ((D) in Figure 17)
- Aging of the mechanical properties of the deposit with time.

Due to the complexity of this process, investigation has mainly been limited to pure salt, mainly calcium carbonate [61,62]. Furthermore, most of the available models describing the crystallization process are based on assumptions and empirical correlations. Simplified models were obtained by considering an average diffusion coefficient of all ions, while diffusion transport of  $H^+$  and  $OH^-$  was neglected. The film theory also was usually adopted to describe the mass transport process. Estimated kinetic expressions of  $CaCO_3$  disposition at low and high  $-pH$  conditions were developed by [72]. Sergev et al. [77] proposed an analytical model that takes into account the kinetics of calcium carbonate deposit formation as well as the diffusional transport of all carbonic ionic species involved in calcium carbonate wall deposition.

Glade et al. [46] and Al-Rawajfeh et al. [71,72,76] investigated the coupling of mass transfer and simultaneous chemical reaction kinetics in the carbonate systems in MSF and MED distillers. They studied the deposition of calcium carbonate and the released rate of Carbon dioxide in a steady regime by developing a model that explained the reactions and mass transfer processes in the bicarbonate system of the brine in MSF distillers [76] and MED distillers [72].

It is recognized that the net deposit rate of scale can be considered as the difference between the total attachment and removal rate of scale according to the following equation:

$$\frac{dm_f}{dt} = \frac{dm_d}{dt} - \frac{dm_r}{dt} \quad (17)$$

where  $\frac{dm_f}{dt}$ ,  $\frac{dm_d}{dt}$  and  $\frac{dm_r}{dt}$  are the net deposit mass rate, the total deposit mass rate, and the removal mass rate per unit area, respectively.

Based on the diffusion transport phenomena, the total mass rate of the specie  $i$  is driven by the difference between the bulk ( $C_b$ ) and interfacial concentration ( $C_{int}$ ).

$$\frac{dm_d}{dt} = K(C_b - C_{int}) \quad (18)$$

where  $K$  is the mass transfer coefficient of the diffusing species.

The rate of the deposition of particles onto the heated surface is governed by the rates of transport of ions from the bulk fluid to the interface and the attachment of the transported species into the crystal layer at the heated surface. According to Bott [5], the mass deposition rate is driven by the concentration between the saturation concentration ( $C_{sat}$ ) and the interfacial concentration ( $C_{int}$ ):

$$\frac{dm_d}{dt} = K_r(C_{int} - C_{sat})^n \quad (19)$$

where  $n$  is reaction order and  $K_r$  is the rate coefficient of the surface reaction that has been shown to depend on temperature according to the Arrhenius equation:

$$K_r = K_0 e^{-E_a / RT_{int}} \quad (20)$$

$K_0$  is the pre-exponential factor,  $E_a$  is the activation energy,  $R$  is the universal gas constant, and  $T_{int}$  is the interfacial temperature.

Knowledge of the form of the crystallization reaction rate ( $n$  in Equation (19)) and the controller mechanism (mass transfer or integration reaction), however crucial to any predictive model of scaling, has been quite limited. Some studies have been conducted by assuming that crystallization fouling is controlled by diffusion rate and/or mass transfer (Equation (18)), surface integration reaction (Equation (19)), or both. Chan and Ghassemi [78] developed a single-species transport model with appropriate boundary condi-

tions to predict calcium carbonate deposition. The  $\text{CaCO}_3$  deposition process was assumed to be controlled by the two processes of mass transport and crystallization reaction on the heat transfer surface.

Other studies [79–81] have proposed that the controller mechanism depends on operating conditions. For laminar flow (low velocity), the mass transfer equation, given in Equation (18), can be used. On the other hand, for forced convection systems (high velocity), mass transfer can be assumed to be the predominant fouling mechanism, and thus, mass deposition rate is considered to be derived by Equation (19). Furthermore, Hasson et al. [82] reported that the crystallization of  $\text{CaCO}_3$  is reaction controlled and proposed the following equation based on the concentrations of  $[\text{Ca}^{2+}]$  and  $[\text{CO}_3^{2-}]$  and the solubility product  $K_{sp}$  of calcium carbonate.

$$\frac{dm_{\text{CaCO}_3}}{dt} = K_r([\text{Ca}^{2+}][\text{CO}_3^{2-}] - K_{sp}) \quad (21)$$

Crystallization fouling of calcium carbonate has been studied extensively, whereas not much attention has been given to other inorganic salts ( $\text{Mg}(\text{OH})_2$ ,  $\text{CaSO}_4$ ) that can participate in scale formation. The mechanisms and thermodynamics of co-precipitation of salts from seawater in MED and MSF plants are poorly understood [61,83,84].

Harris et al. [84] studied the formation of magnesium scale in seawater distillation plants. They proposed that scale formation occurs via the thermal decomposition of the hydrogen carbonate ion to carbonate ion and hydroxyl ion and that hydromagnesite precipitates in the first step to calcium carbonate.

Al-Rawajfeh et al. [76] improved the work of Al-Rawajfeh [71] to consider mixed salt precipitation in once-through and brine recycle MFS processes (MSF-OT and MSF-BR). They included the deposition of calcium sulfate with calcium carbonate in their fouling model. However, their model only considered the rate of deposition of scale. Glade et al. [46] conducted different test rigs in a wide range of process conditions. In experiments with seawater, the metal tube surfaces in the falling film evaporator were covered with a two-layer scale comprising a thin layer of flaky magnesium-rich under a thick layer of calcium carbonate crystals.

Most recently, Alsadaie and Mujtaba [59,83] developed a dynamic fouling model to predict the rate of crystallization of calcium carbonate ( $\text{CaCO}_3$ ) and magnesium hydroxide ( $\text{Mg}(\text{OH})_2$ ) in MSF-OT. To calculate the crystal growth of magnesium hydroxide, they used Equation (23) proposed by [85]. In addition, the removal rate mechanism was proposed in Equation (24). The removal rate equation is a function of various parameters (wall stress of the bulk flow,  $\tau_f$ , shear strength of the fouling layer,  $\sigma_f$  and density of the fouling layer,  $\rho_f$ ). The proposed fouling model takes into account the kinetic reaction and mass diffusion of calcium carbonate and magnesium hydroxide. The results indicated that the crystallization of both salts strongly depends on the top brine temperature (TBT), velocity, and salinity.

$$\frac{dm_{\text{Mg}(\text{OH})_2}}{dt} = K_r\{([\text{Mg}^{2+}][\text{OH}^-])^{1/3} - [K_{sp}]^{1/3}\} \quad (22)$$

where  $K_{sp}$  is the solubility product for magnesium hydroxide.

$$\frac{dm_r}{dt} = K_{rem} \frac{\tau_f}{\sigma_f} \left( \frac{\mu_w g}{\rho_w} \right)^{1/3} \quad (23)$$

where  $K_{rem}$  is the removal rate constant. The thermal resistance of the fouling layer  $R_f$ , can be determined by the following equation [86]:

$$\frac{dR_f}{dt} = \frac{1}{\lambda_f \rho_f} \frac{dm_f}{dt} \quad (24)$$

where  $\lambda_f$  the thermal conductivity of the fouling layer and  $\rho_f$  is the density of the layer.

### 3.3. Prediction of Scaling Potential in Thermal Desalination

#### 3.3.1. LSI, RSI, and SI, Index

For the highly simplified model of water containing only CO<sub>2</sub> and calcium carbonate, three indices: the Langelier Saturation Index (LSI) (ASTM D3739-06 and ASTM4582-05), the Ryznar Stability Index (RSI), and supersaturation index (SI) have been introduced to predict the scaling tendency of an aqueous solution [87]. The two indexes, LSI and RSI, are based upon a calculated pH of saturation for calcium carbonate (pH<sub>s</sub>). The pH<sub>s</sub> value is then used in conjunction with the actual pH of seawater to calculate the value of the index as follows [87]:

$$LSI = pH - pH_s \quad (25)$$

$$RSI = 2 pH_s - pH \quad (26)$$

with pH as the actual pH value and pH<sub>s</sub> as the pH value of calcium carbonate saturation given by:

$$pH_s = (pK_2 - pK_{sp}) + pTA + p[Ca^{2+}] \quad (27)$$

where K<sub>2</sub> is the second dissociation constant of carbonic acid. The p function indicates the negative logarithm of that variable.

A positive LSI indicates that the solution is supersaturated with calcium carbonate and the water has the potential to form scale. Conversely, for a solution with a negative LSI, the solution is under saturated conditions and is potentially corrosive.

It should be noted that experimental values of RSI are in good concordance with calculated values. Accordingly, the RSI is used in many applications [61]. An interpretation of the RSI is given in Table 1. In addition to LSI and RSI indices, the supersaturation index (SI) defined as follows can be used [88]:

$$SI = \frac{I_{AP}}{K_{sp}} \quad (28)$$

where I<sub>AP</sub> is the ion activity product and K<sub>sp</sub> is the solubility product of organic scale such as CaCO<sub>3</sub>, CaSO<sub>4</sub>, BaSO<sub>4</sub>, and SiO<sub>2</sub>. An SI index greater than unity indicates that the solution is supersaturated and the water has the potential for scale formation.

**Table 1.** Interpretation of the RSI [66].

RSI Value	Indication
4.0–5.0	Severe scaling
5.0–6.0	Slight Scaling
6.0–7.0	Stable water
7.0–7.5	Dissolving of scale and corrosive
7.5–9.0	Intense dissolving of scale and corrosion
>9.0	Very intense dissolving of scale and corrosion

#### 3.3.2. Fouling Factor Resistance Calculation

The scale deposition on surface tubes may lead to some increase in the fouling resistance and decrease in the heat flux and, hence, affects the plant performance defined by the Gain output ratio (GOR) as well as plant production rate. Since the fouling accumulation rate is quite difficult to predict, usually a fouling factor (FF) was calculated and monitored during the operation of the desalination plant based on the following equation:

$$FF = \frac{1}{U(t)} - \frac{1}{U_c} \quad (29)$$

where U(t) is the overall heat transfer coefficient at any given time (t) and U<sub>c</sub>(t) is overall heat transfer coefficients under a clean state.

Many experimental studies on the performance of MED and MSF plants at high temperatures with real seawater were conducted to evaluate the viability of the technology

at high-temperature operation for scale and corrosion issues [48,68,89,90]. In most cases, evaluation tests of MSF or MED desalination plants were carried out by monitoring FF resistance, visual inspection of tube bundles, and analysis of the chemical scale of brine.

#### 4. Fouling Estimation and Prediction

In the previous sections, we reviewed the main aspects of the formation mechanism of fouling, which is very important to be considered in the process design phase to reduce the fouling accumulation in the heat exchangers. After the process is online, fouling conditions estimation and prediction is an important step to assess the current health of the heat exchanger and help the maintenance team toward an optimum maintenance plan in order to avoid unnecessary or unplanned shutdowns. There are two main types of fouling monitoring approaches, the instrument-based approach and the model-based approach. The former approach is limited because it requires special sensors to be installed, which is usually available for complicated boilers. On the other hand, the model-based approach utilizes existing measurements only to estimate and predict fouling rate/resistance, which makes it more widely used, especially with the availability of sophisticated data analytics and computing power in modern systems. The model-based approach can be divided into three categories: deterministic models, which are derived from first principles; semi-empirical models based on first principles with unknowns that are estimated using a parameter estimation technique; and artificial intelligence models [91].

One of the early deterministic models to describe fouling was presented in 1959 by Kern and Seaton [26], where they stated that the rate of change in deposition mass could be defined as Equation (5).

Taking into consideration tubular flow patterns, the change in fouling thickness ( $x_f$ ) can be presented as:

$$\frac{dx_f}{dt} = K_1cM - K_2\tau x_{ft} \tag{30}$$

where  $c$  is the concentration of fouling,  $M$  represents the mass flow rate,  $K_1$  and  $K_2$  are real constants,  $\tau$  is the shear stress and  $x_{ft}$  is the thickness of the fouling layer at time  $t$ . In Equation (30), on the right side, the first term denotes the deposition rate, while the second term denotes the erosion or removal rate. The Kern model is considered a general model for fouling description. Based on this approach, many models have been proposed [8]. Table 2 highlights some of these models, which are mainly developed for crude oil. A more detailed discussion can be found in [8,92].

**Table 2.** Crude oil fouling prediction models.

Model	Equation
Ebert and Panchal [91]	$\frac{dR_f}{dt} = \alpha Re^\beta \exp\left(-\frac{E}{R_g T_f}\right) - \gamma \tau_w$
Polley et al. [93]	$\frac{dR_f}{dt} = \alpha Re^{-0.8} Pr^{-0.33} \exp\left(-\frac{E}{R_g T_s}\right) - \gamma Re^{0.8}$
Nasr and Givi [94]	$\frac{dR_f}{dt} = \alpha Re^{-0.8} \exp\left(-\frac{E}{R_g T_f}\right) - \gamma Re^{0.4}$
Shetty et al. [95]	$\frac{dR_f}{dt} = \alpha Re^\beta Pr^{-0.33} \exp\left(\frac{-E}{RT_{eff}}\right) - \gamma \tau_w$ $T_{eff} = \alpha_1 T_{so} + \alpha_2 T_b$

The parameters ( $\alpha, \beta, E, \gamma$ ) are to be chosen according to specifications of the crude oil [96].

Markowski et al. [97] presented an algorithm for the determination of fouling resistance used for two series-connected shell and tube heat exchangers. The least square method was used to adjust the surface film conductances for both the shell side and tube side, which were given by the empirical equation for the Nusselt number defined by Equation (31):

$$Nu = C \cdot Re^a Pr^b (Pr/Pr_w)^o \tag{31}$$

where  $Re$  is Reynolds number and  $Pr$  is Prandtl number and  $a, b, C, O$  are constants.

The method developed by Markowski et al. [98] requires that the data on mass flow rate, temperature, pressure, and thermophysical properties are continuously available. The objective functions to be minimized are defined as the difference between the outlet temperatures obtained from the mathematical model and the measured temperatures as written in Equation (32).

$$Objective\ Function = \sum_{j=1}^n \left[ \left( T_{to\_mod(j)} - T_{to\_measured(j)} \right)^2 + \left( T_{so\_mod(j)} - T_{so\_measured(j)} \right)^2 \right] \tag{32}$$

The suggested method was validated using operational records of an industrial shell and tube heat exchanger paired with a crude distillation unit.

A fouling detection approach based on observer for bilinear systems is proposed by Deltrot et al. [99], where a simplified distributed model is used to construct the heat exchanger nonlinear state-space model, as shown in Figure 18. Real experimental data obtained from a laboratory were used for model validation.

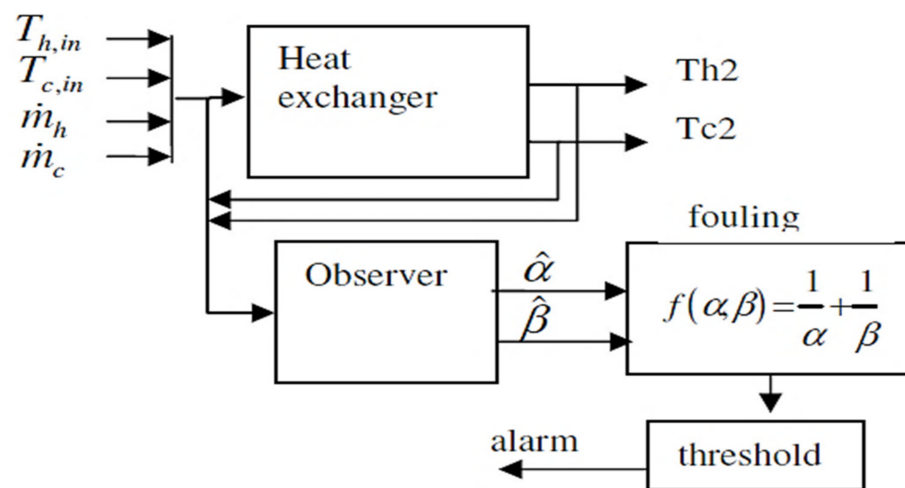


Figure 18. A nonlinear observer diagram [99].

An extended Kalman filter was suggested by Jonsson et al. [98] for fouling detection, where a lumped nonlinear state-space model utilized to model a counter-flow plate heat exchanger was used. CFD software used for system simulation considered mass flow rates, outlet temperatures, and inlet temperatures as the input. Sivathanu and Subramanian [100] proposed a dual-extended Kalman filter approach to estimate the parameters that affect fouling in the reheater of a power plant. They used a performance index, namely, a cleaning factor, to monitor the performance of the heat exchanger.

Delrot et al. [101] presented a Takagi–Sugeno approach [102] for fouling detection in a counterflow tubular heat exchanger where the fuzzy observer is designed according to the physical model obtained by dividing the heat exchanger into multiple sections and finding the lumped model for each section. ANSYS fluent was used to simulate fouling by changing the thermal conductivity of the inner tube. The developed observer showed good sensitivity toward fouling detection and did not impose that the system should be in a steady state.

Sun, Saqi, and Xie [103] proposed a model that predicts fouling resistance based on a relevance vector machine with a wavelet kernel where the model is trained using experimental data. A semi-empirical model was adopted for fouling detection in [104] by Dragan, where a linear model with unknown parameters is derived from first principles, then the least squared method (LSM) was deployed for estimation of the unknowns. Gudmundsson [105] compared different detection techniques, including the Kalman filter, extended Kalman filter, NTU, fuzzy observers, and ANN applied for cross-flow and counter-

flow heat exchangers. Gudmundsson outlined that these techniques-based detection methods are efficient in detecting fouling early; however, their implementations require high computational costs.

A lock-in semi-empirical technique for fouling detection was proposed by Andrjesdóttir et al. [106]. The technique was based on the lock-in amplifier channels theory, which is used for noise attenuation in signal processing applications. Based on plate and frame heat exchangers, a numerical model was developed, and experimental data were used for validation. The obtained results showed that the proposed technique had a high sensitivity in addition to its ability to differentiate between the effect of a decrease in mass flow rate and fouling effect. Lalot et al. [107] applied this technique numerically by injecting a small perturbation in the inlet temperature of the side where the fouling was expected to occur using an electrical heater, as shown in Figure 19, where the temperature changed in a periodical manner. Considering the parallel flow plate and frame heat exchanger as a case study, the obtained results illustrated that a window of four million samples was appropriate for accurate fouling detection.

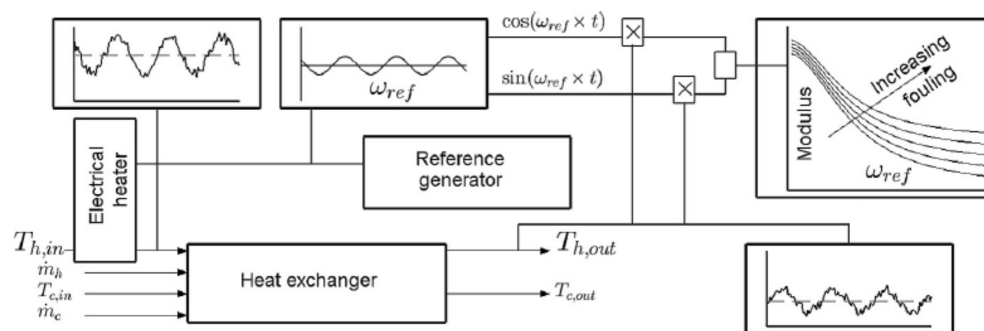


Figure 19. Implementation of a lock-in technique [107].

A distributed dynamic semi-empirical model was proposed by Coletti and MacChietto [108] for a tube-side fouling prediction taking into account the change in fluid properties due to temperature, heat exchanger geometric parameters, and variation in the fouling accumulation with time where the model could capture the spatial and temporal variation of the system states. The model was validated with a practical data set taken from a crude oil refinery where the model showed an error of less than 2% for a one-year-ahead prediction.

AlHadad, Schick, and Maillet [109] proposed a detection technique based on the variation of the heat exchanger thermal impulse responses where the system impulse response was firstly identified at the clean state and then under operation assuming that the model was time-invariant, linear, and under steady-state operation. A shell and tube heat exchanger model was simulated using COMSOL software, where the impulse response was identified by injecting a thermal disturbance in the hot side of the heat exchanger through a surface heat source and then measuring the responses of outlet temperatures. The results showed that this method was sensitive to changes in fouling.

Radhakrishnan et al. [110] proposed an ANN model to predict outlet temperatures of shell and tube heat exchangers. ANN is trained based on historical plant data using feedforward and recurrent neural network architectures, where the latter showed a better prediction accuracy. Forty-four features were considered initially for model development and then reduced to twenty-five features using principal component analysis (PCA) and partial least squares (PLS) techniques. The cleaning process could be scheduled according to the decrement in the efficiency of heat transfer based on predicted values of temperatures. Still, the developed model showed poor generalization capability.

Based on experimental data sets gathered from the literature, Davoudi and Valeri [111] developed an ANN fouling prediction model using a shallow neural network with ten hidden neurons where fluid properties and time were considered as input to the ANN

while fouling factor was the output. The model showed a small prediction error with a mean square error (MSE) of 0.0013.

A fouling detection method based on Elman NN, depicted in Figure 20, was proposed by Wang et al. [112]. The weights of the NN were optimized using a genetic algorithm. An experiment was conducted to simulate the formation of calcium carbonate ( $\text{CaCO}_3$ ) fouling in a shell and tube heat exchanger where a self-designed setup captured the experimental data of fouling resistance, pH, and dissolved oxygen used for NN training. The detection method showed a total error of 8.78%.

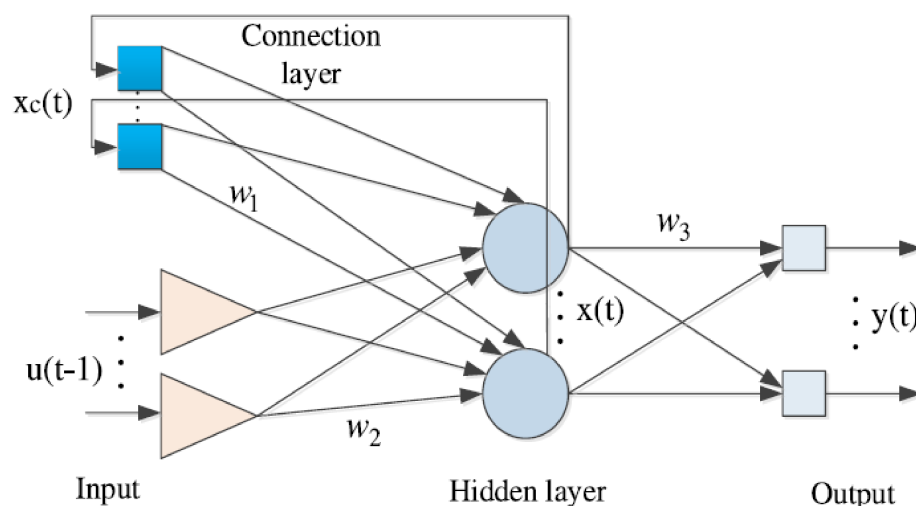


Figure 20. Elman Neural Network architecture [112].

Aminian and Shahhosseini [113] employed ANN to develop a set of mathematical formulations that can be used to predict fouling behavior, which is very helpful in avoiding operating conditions that accelerate fouling.

Al-Naser et al. [114] presented an artificial intelligence approach for fouling estimation and prediction. The approach was divided into stages; the first one was to estimate FF using ANN, while the second approach used the Long Term Short Memory (LSTM) approach to predict fouling in shell and tube heat exchangers. Process data were generated using the KBC PetroSIM process simulator, and simulation was performed using MATLAB showing high prediction accuracy with a mean square error (MSE) of  $8.5 \times 10^{-11}$  and a root-mean-square error (RMSE) of  $1.72 \times 10^{-6}$  for estimation and fouling prediction, respectively.

Another study conducted by Al-Naser et al. [115] added another analysis element in performance monitoring. In this study, not only the overall value of FF was estimated, but it could provide an estimate of the local fouling value inside the heat exchanger. In this study, a heat exchanger model with five segments was built using PetroSIM to simulate different fouling scenarios wherein one segment was fouled at a time. Then, tube outlet temperature, tube pressure drop, and shell outlet temperature were used to build artificial models that determined which segment was most likely fouled. A similar study was conducted by Schlüter et al. [116] to determine local fouling resistance with the help of fiber sensors, which provided temperature measurements along a double-pipe heat exchanger to correct local fouling resistance values.

For phase change heat exchangers, there are only a few fouling analysis studies. For example, Grosfils et al. [117] proposed a system for monitoring fouling in thermosiphon reboilers based on a static model of the fouling resistance. He developed a grey box model to monitor tube fouling resistance with only two unknown parameters to be estimated at steady-state conditions. He used data from an industrial boiler to validate the model showing a good estimation of fouling evolution without having been affected by set point changes in vapor flow, as an automatic detection algorithm was used to eliminate transient data. Yamashita [118] used a combination of a theoretical model-based approach and a

data-driven approach to bypass the problem of the non-availability of several process measurements. They introduced a method that monitored fouling in a thermosiphon reboiler in a simulated debutanizer column and a method to estimate the fouling resistance. PLS regression was successfully used to model the tube-side film heat transfer coefficient, where its estimated results agreed with their measurements, while the overall heat transfer coefficient and heat flux were modeled using a physical model.

Kuwahara et al. [119] proposed a method that computed the actual fouling resistance in a thermosiphon reboiler from measurable process data only with the help of dimensional analysis. They used the monitored fouling rate for estimating the parameters of a simplified Ebert–Panchal model, which was used to predict future fouling behavior with specified conditions of operation. In the end, they concluded that the fouling rate could be decreased solely by controlling the steam flow rate.

## 5. Fouling Mitigation

Several strategies, including chemical, mechanical, and physical ones, have been used in recent years to solve the fouling problems in heat exchanger systems.

Numerous chemical additives have been developed and are currently being used commercially to reduce crystallization fouling, chemical reaction fouling, particle fouling, etc. Inhibitors, antiscalants, acids, and other suitable additives are typically added to fouling solutions under working conditions. These additives may react in various ways (such as sequestering agents, threshold agents, crystal modifiers, and dispersants) to stop scaling, get rid of whatever fouling has already been deposited on heat exchanger surfaces, or slow down chemical fouling reactions [74]. Engineers and operators prefer the chemical method for cleaning fouled heat exchangers. However, it has several drawbacks, such as a high operating cost and risk to equipment safety and the environment [24,74].

In addition to the aforementioned chemical treatments, a number of mechanical techniques have recently been researched and developed for fouling control and mitigation. Based on their functioning and the types and features of fouling, these techniques can be divided into two groups: (i) brute force methods, such as high-pressure jets, lances, drills, and scrapers, and (ii) mild methods, such as sponge balls, brushes, sonic horns, vibrators, etc. [24]. Mechanical procedures are widely utilized in severe fouling situations because of their simplicity and capacity to remove fully hard scale deposited on heat exchanger surfaces.

Fouling removal can also be accomplished using other effective cleaning techniques, such as thermal shock, electromagnetic water treatment, and UV radiation [120].

In addition to cleaning techniques, increasing the thermal efficiency of heat exchangers is another option for reducing fouling. It can be accomplished by modifying surface features and adjusting process operating conditions. Increased fluid flow rate or velocity causes high shear stress across the heat transfer surface, which enhances the efficiency of the heat exchanger, according to Awais and Bahuiyan [24]. The deposit of foulants can be reduced by adding electronic antifouling, fibers, and catalytic materials to the fouling solution [23,24].

According to the findings from several researchers [3,5,23,24,74], a lower fouling rate can also be attained by taking into account heat exchanger design features and parameters, which can be summarized as follows:

- Over-sizing heat transfer area;
- Smoothing surfaces of heat exchangers;
- Increasing thermal conductivity of material surfaces;
- Inserting turbulence promoters or making corrugated surfaces;
- Including different types and patterns of fins;
- Using fluidized-bed heat exchangers;
- Using nanomaterials as surface coatings.

Awais and Bhuiyan conducted a review [24] on recent advancements in fouling mitigation and control in heat exchanger systems. They discussed the effect of different

designs and operating parameters on the formation of fouling. They concluded that the mass flow rate, the temperature variation, and material surfaces are the main parameters that should be considered in the design and operation of heat exchangers.

## 6. Available Industrial Solutions

In industry, there are several solutions implemented in the field to monitor heat exchanger performance and predict its failure, which helps in improving maintenance planning and process efficiency. There are several technologies that have been utilized, ranging from basic heat exchanger equations, advanced analytics, and machine learning to the Industrial Internet of Things (IIoT), as well as edge and cloud computing.

For example, Siemens has HeatXchMon, which is a condition-based predictive maintenance solution that is used mainly for shell and tube heat exchangers. This solution uses an intelligent approach to make the comparison between measured values and the characteristic surfaces of the heat exchanger calculated by simulations of clean and fouled states based on the technical specifications of the heat exchanger [121]. Yokogawa utilizes IIoT technology for Real-Time Condition Monitoring for Heat Exchangers with IIoT [122] in which sensors monitor the effectiveness of the process heat exchanger. The end-user can add wireless sensors to monitor heat exchanger performance. By monitoring the inlet and outlet temperature, the operators have a better view of heat exchanger performance. Therefore, the fouling will be visible over time if it occurs. Additionally, there is another solution from Yokogawa, i.e., Field Asset Analytics (InsightSuiteAE), which can evaluate shell and tube heat exchanger health [123]. KBC, which is a Yokogawa company, has a solution called Hx Monitor which is intended mainly for Heat Exchanger Network (HEN) monitoring. It is an effective tool to determine which heat exchanger should be cleaned and when the cleaning should be performed. Thus, this tool can be used to optimize the maintenance schedule for heat exchanger equipment maintenance and enhance plant operations [124]. Emerson has a heat exchanger monitoring solution that combines the heat exchanger process and best practices into the software using dynamic readings from wire and wireless instrumentation along with heat transfer calculations, which help the operation team to predict the performance of the heat exchanger [125]. It also has another solution called Plantweb Performance Advisor that can monitor heat exchangers, condensers, and boilers [126]. ABB has a system 800x A Heat Exchanger Asset Monitor (HXAM) solution to notify the operation team about the decline of heat exchanger performance due to fouling or a major change in the operating point [127]. Honeywell has Forge Asset Performance Management (APM) which is an advanced predictive analytics solution that can monitor heat exchanger performance, including FF and fouling percentage [128]. GE utilizes artificial intelligence, edge analytics, and digital twin to empower asset analytics, including heat exchanger performance monitoring [129,130]. GS Caltex also utilizes a digital twin and uses a model-based monitoring solution for monitoring fouling in heat exchangers [131].

## 7. Conclusions and the Future

Fouling analysis is very useful for improving process efficiency, reducing costs, and avoiding plant shutdowns. This paper addresses key aspects of fouling and approaches used for fouling analysis in heat exchangers.

- In terms of modeling, this paper gives an overview of fouling models used for single-phase heat exchangers. In addition, it discusses experimental and numerical approaches to multiphase flow fouling modeling with a focus on the thermal desalination process, which usually suffers from fouling.
  - Fouling models and correlations are categorized into seven types: enhanced models, nucleate boiling models, superposition models, asymptotic models, largest mechanism predominant models, flow pattern-based models, and hybrid models.
- In terms of fouling prediction, this paper discusses the methods used for it, which are very important to optimize heat exchanger maintenance and cleaning plans.

- Models used for fouling rate estimation and prediction can be categorized into the following three main types: deterministic models, semi-empirical models, and artificial intelligence models.
- However, the literature shows that there is a need for more research in the area of multiphase flow heat exchangers to improve the accuracy of fouling analysis results, which could lead to the more practical implementation of the methods used for fouling estimation and prediction.

In the future, the work can be extended by focusing on fouling in membrane-based desalination technologies such as RO and ED for the purpose of comparison with phase change desalination technologies, which may result in simpler models. Furthermore, to understand fouling better and find solutions, it is recommended to broaden our search into natural systems and focus on how these cope with such situations, as biomimetics has been known to solve or improve complex human problems.

**Author Contributions:** Conceptualization, R.B.-M., S.E.-F. and M.A.-N.; methodology, R.B.-M., S.E.-F.; investigation, R.B.-M., S.E.-F., M.A.-N., B.A.Q., M.A.M.E., A.A., F.A.-S. and R.B.M.; R.B.-M., S.E.-F. and M.A.-N.; data curation; writing—original draft preparation, R.B.-M., S.E.-F., M.A.-N., B.A.Q., M.A.M.E., A.A., F.A.-S. and R.B.M.; writing—review and editing, R.B.-M., S.E.-F., M.A.-N., B.A.Q., M.A.M.E., A.A., F.A.-S. and R.B.M.; supervision, R.B.-M. project administration, R.B.-M., S.E.-F.; funding acquisition, R.B.-M., S.E.-F. and M.A.-N. All authors have read and agreed to the published version of the manuscript.

**Funding:** This research was funded by King Fahd University of Petroleum and Minerals and Yokogawa KSA under grant SE002487.

**Acknowledgments:** The authors would like to acknowledge King Fahd University of Petroleum and Minerals and Yokogawa KSA for their support and funding under grant SE002487.

**Conflicts of Interest:** The authors declare no conflict of interest.

## References

1. Murshed, S.M.S.; Lopes, M.M.; Murshed, S.M.S.; Lopes, M.M. *Heat Exchangers—Design, Experiment and Simulation*; InTech: London, UK, 2017. [CrossRef]
2. Müller-Steinhagen, H.; Malayeri, M.R.; Watkinson, A.P. Heat Exchanger Fouling: Mitigation and Cleaning Strategies. *Heat Transf. Eng.* **2011**, *32*, 189–196. [CrossRef]
3. Abd-Elhady, M.S.; Malayeri, M.R. Transition of convective heat transfer to subcooled flow boiling due to crystallization fouling. *Appl. Therm. Eng.* **2016**, *92*, 122–129. [CrossRef]
4. Shell & Tube Heat Exchanger Cleaning. Apex Engineering Products. Available online: <https://www.apexengineeringproducts.com/shell-and-tube-heat-exchanger-cleaning/> (accessed on 8 January 2023).
5. Bott, T.R. *Fouling of Heat Exchangers*; Elsevier Science: Amsterdam, The Netherlands, 1995. [CrossRef]
6. Jradi, W.B.R.; Marvillet, C.; Jeday, M.R. *Fouling in Industrial Heat Exchangers: Formation, Detection and Mitigation*; InTech: London, UK, 2022; Volume 11, p. 13. [CrossRef]
7. Hale, M. Types of heat exchanger fouling. *World Pumps* **2021**, *2021*, 20–22.
8. Ajayi, O.; Ogbonnaya, S.K. Fouling phenomenon and its effect on heat exchanger: A review. *Front. Heat Mass Transf.* **2017**, *9*, 1–12. [CrossRef]
9. García, S.; Trueba, A. Fouling in Heat Exchangers. In *Inverse Heat Conduction and Heat Exchangers*; InTech: London, UK, 2019. [CrossRef]
10. Hewitt, G.F.; Shires, G.L.; Bott, T.R. *Process Heat Transfer*; CRC Press/Begell House: Boca Raton, FL, USA, 1994.
11. Master, B.I.; Chunangad, K.S.; Pushpanathan, V. Fouling Mitigation Using Helixchanger Heat Exchangers. *Heat Exch. Fouling Clean. Fundam. Appl.* **2003**, *317*, 1–6.
12. Economic Impact of Fouling in Heat Exchangers. Available online: <https://www.watco-group.co/fouling-impact-economical/> (accessed on 15 January 2021).
13. Crittenden, B.D. Chemical Reaction Fouling of Heat Exchangers. *Fouling Sci. Technol.* **1988**, *145*, 315–332. [CrossRef]
14. Khairansyah, M.D.; Biyanto, T.R. Economical Aspect of Heat Exchanger Cleaning Affected by Fouling. *Int. Semin. Sci. Technol.* **2015**, *2*, 27–28.
15. Akinc, H.E.; Becer, M.; Bakir, M.; Ozcelik, Y.; Balkan, F. Fouling monitoring in crude oil preheat trains. In *Proceedings of the Heat Exchanger Fouling and Cleaning, Budapest, Hungary, 9–14 June 2013*; Volume 2013, pp. 18–21.

16. Bories, M.; Patureauux, T. Preheat Train Crude Distillation Fouling Propensity Evaluation by the Ebert and Panchal Model. *Heat Exch. Fouling Clean. Fundam. Appl.* 2003. Available online: [http://dc.engcon\\_ntl.org/heatexchanger/27](http://dc.engcon_ntl.org/heatexchanger/27) (accessed on 11 December 2022).
17. Müller-Steinhagen, H.; Malayeri, M.R.; Watkinson, A.P. Fouling of Heat Exchangers—New Approaches to Solve an Old Problem. *Heat Transf. Eng.* 2005, 26, 1–4. [[CrossRef](#)]
18. Macchietto, S.; Hewitt, G.F.; Coletti, F.; Crittenden, B.D.; Dugwell, D.R.; Galindo, A.; Jackson, G.; Kandiyoti, R.; Kazarian, S.G.; Luckham, P.F.; et al. Fouling in Crude Oil Preheat Trains: A Systematic Solution to an Old Problem. *Heat Transf. Eng.* 2011, 32, 197–215. [[CrossRef](#)]
19. Kondyli, A.; Schrader, W. Study of Crude Oil Fouling from Sulfur-Containing Compounds Using High-Resolution Mass Spectrometry. *Energy Fuels* 2021, 35, 13022–13029. [[CrossRef](#)]
20. Melo, L.F.; Bott, T.R.; Bernardo, C.A. *Fouling Science and Technology*; Springer: Dordrecht, The Netherlands, 1988. [[CrossRef](#)]
21. Kuruneru, S.T.W.; Vafai, K.; Sauret, E.; Gu, Y. Application of porous metal foam heat exchangers and the implications of particulate fouling for energy-intensive industries. *Chem. Eng. Sci.* 2020, 228, 115968. [[CrossRef](#)]
22. Heu, C.S.; Jang, H.; Jeon, J.; Lee, K.-S.; Kim, D.R. Recent progress on developing anti-frosting and anti-fouling functional surfaces for air source heat pumps. *Energy Build.* 2020, 223, 110139. [[CrossRef](#)]
23. Idumah, C.I.; Obele, C.M.; Emmanuel, E.O.; Hassan, A. Recently Emerging Nanotechnological Advancements in Polymer Nanocomposite Coatings for Anti-corrosion, Anti-fouling and Self-healing. *Surf. Interfaces* 2020, 21, 100734. [[CrossRef](#)] [[PubMed](#)]
24. Awais, M.; Bhuiyan, A.A. Recent advancements in impedance of fouling resistance and particulate depositions in heat exchangers. *Int. J. Heat Mass Transf.* 2019, 141, 580–603. [[CrossRef](#)]
25. Wen, X.; Miao, Q.; Wang, J.; Ju, Z. A multi-resolution wavelet neural network approach for fouling resistance forecasting of a plate heat exchanger. *Appl. Soft Comput.* 2017, 57, 177–196. [[CrossRef](#)]
26. Kern, D.Q.; Seaton, R.E. A theoretical analysis of thermal surface fouling. *Br. Chem. Eng.* 1959, 4, 258–262.
27. Liu, X.; Zhang, X.; Lu, T.; Mahkamov, K.; Wu, H.; Mirzaeian, M. Numerical simulation of sub-cooled boiling flow with fouling deposited inside channels. *Appl. Therm. Eng.* 2016, 103, 434–442. [[CrossRef](#)]
28. Helalizadeh, A.; Müller-Steinhagen, H.; Jamialahmadi, M. Mixed salt crystallisation fouling. *Chem. Eng. Process. Process Intensif.* 2000, 39, 29–43. [[CrossRef](#)]
29. Haghshenasfard, M.; Yeoh, G.H.; Dahari, M.; Hooman, K. On numerical study of calcium sulphate fouling under sub-cooled flow boiling conditions. *Appl. Therm. Eng.* 2015, 81, 18–27. [[CrossRef](#)]
30. Pääkkönen, T.; Riihimäki, M.; Simonson, C.; Muurinen, E.; Keiski, R. Crystallization fouling of CaCO<sub>3</sub>—Analysis of experimental thermal resistance and its uncertainty. *Int. J. Heat Mass Transf.* 2012, 55, 6927–6937. [[CrossRef](#)]
31. Mayer, M.; Bucko, J.; Benzinger, W.; Dittmeyer, R.; Augustin, W.; Scholl, S. The impact of crystallization fouling on a microscale heat exchanger. *Exp. Therm. Fluid Sci.* 2012, 40, 126–131. [[CrossRef](#)]
32. Jamialahmadi, M.; Müller-Steinhagen, H. Scale Formation During Nucleate Boiling—A Review. *Corros. Rev.* 1993, 11, 25–54. [[CrossRef](#)]
33. Esawy, M. Fouling of Structured Surfaces during Pool Boiling of Aqueous Solutions. Ph.D. Thesis, University of Stuttgart, Stuttgart, Germany, 2011.
34. Fang, X.; Zhuang, F.; Chen, C.; Wu, Q.; Chen, Y.; He, Y. Saturated flow boiling heat transfer: Review and assessment of prediction methods. *Heat Mass Transf.* 2018, 55, 197–222. [[CrossRef](#)]
35. Chen, J. A correlation for boiling heat transfer to saturated fluids in convective flow. *Ind. Eng. Chem. Process Des. Dev.* 1966, 5, 322–329. [[CrossRef](#)]
36. Yoon, S.H.; Cho, E.S.; Hwang, Y.W.; Kim, M.S.; Min, K.; Kim, Y. Characteristics of evaporative heat transfer and pressure drop of carbon dioxide and correlation development. *Int. J. Refrig.* 2004, 27, 111–119. [[CrossRef](#)]
37. Fang, X.; Wu, Q.; Yuan, Y. A general correlation for saturated flow boiling heat transfer in channels of various sizes and flow directions. *Int. J. Heat Mass Transf.* 2017, 107, 972–981. [[CrossRef](#)]
38. Esawy, M.; Malayeri, M.R.; Müller-Steinhagen, H. Mechanism of crystallization fouling during pool boiling of finned tubes. In Proceedings of the 13th International Water Technology Conference, Hurghada, Egypt, 11–13 March 2009.
39. Bornhorst, A.; Müller-Steinhagen, H.; Zhao, Q. Reduction of Scale Formation Under Pool Boiling Conditions by Ion Implantation and Magnetron Sputtering on Heat Transfer Surfaces. *Heat Transf. Eng.* 1990, 20, 6–14. [[CrossRef](#)]
40. Fukada, Y.; Haze, I.; Osakabe, M. The effect of fouling on nucleate pool boiling of small wires. *Heat Transf.* 2004, 33, 316–329. [[CrossRef](#)]
41. Freeborn, J.; Lewis, D. Initiation of Boiler Scale Formation. *J. Mech. Eng. Sci.* 1962, 4, 46–52. [[CrossRef](#)]
42. Wang, J.; Xu, Z.; Han, Z.; Zhao, Y. Effect of heat flux and inlet temperature on the fouling characteristics of nanoparticles. *Chin. J. Chem. Eng.* 2018, 26, 623–630. [[CrossRef](#)]
43. Taler, D.; Trojan, M.; Taler, J. Mathematical modelling of tube heat exchangers with complex flow arrangement. *Chem. Process. Eng.* 2011, 32, 7–19. [[CrossRef](#)]
44. GWI. *IDA Desalination Yearbook 2017–2018*; Media: Oxford, UK, 2017.
45. Gill, J.S. A novel inhibitor for scale control in water desalination. *Desalination* 1999, 124, 43–50. [[CrossRef](#)]

46. Glade, H.; Krömer, K.; Will, S.; Detering, J.; Essig, M.; Kempter, A.; Stephan Nied, G.S. On scale formation of magnesium salts in thermal seawater desalination. In Proceedings of the World Congress—Perth Convention and Exhibition Centre (PCEC), Perth, WA, Australia, 4–9 September 2011.
47. Al-Sofi, M.A.K.; Flash, S.; Distillers, M.S.F. Fouling phenomena in multi stage flash (MSF) distillers. *Desalination* **1999**, *126*, 61–76. [[CrossRef](#)]
48. Darwish, M.A.; El-Refae, M.M.; Abdel-Jawad, M. Developments in the multi-stage flash desalting system. *Desalination* **1995**, *100*, 35–64. [[CrossRef](#)]
49. Amjad, Z. Scale inhibition in desalination applications: An overview. In Proceedings of the NACE—International Corrosion Conference Series, Denver, CO, USA; 1996; pp. 1–26.
50. Zhao, X.; Chen, X.D. A Critical Review of Basic Crystallography to Salt Crystallization Fouling in Heat Exchangers. *Heat Transf. Eng.* **2013**, *34*, 719–732. [[CrossRef](#)]
51. McCutchan, J.W. *Scale Control in Saline Water Evaporators—A Review of Current Status*; U.S. Department of the Interior: Washington, DC, USA, 1969.
52. El Din, A.S.; El-Dahshan, M.; Mohammed, R. Scale formation in flash chambers of high-temperature MSF distillers. *Desalination* **2005**, *177*, 241–258. [[CrossRef](#)]
53. Mubarak, A. A kinetic model for scale formation in MSF desalination plants. *Effect of antiscalants*. *Desalination* **1998**, *120*, 33–39. [[CrossRef](#)]
54. Stephan, K. Heat Transfer in horizontal Falling Film Evaporators. In Proceedings of the IDA World Congress, Dubai, United Arab Emirates; 2009; pp. 1–10. [[CrossRef](#)]
55. Al-Anezi, K.; Hilal, N. Scale formation in desalination plants: Effect of carbon dioxide solubility. *Desalination* **2007**, *204*, 385–402. [[CrossRef](#)]
56. Hamrouni, B.; Dhahbi, M. Thermodynamic description of saline waters—Prediction of scaling limits in desalination processes. *Desalination* **2001**, *137*, 275–284. [[CrossRef](#)]
57. Mahmoud, A.M.; Kim, Y.; Ben Mansour, R.; Al-Aithan, A.; Lee, Y.; Ahmed, S.; Varshney, H.; Chung, H.; Bamardouf, K.; Hamed, O.A.; et al. Experimental analysis and techno-economic study of once through long tube MSF desalination plants. *Desalination Water Treat.* **2017**, *73*, 137–144. [[CrossRef](#)]
58. Rosen, M.; Farsi, A. *Sustainable Energy Technologies for Seawater Desalination*; Elsevier: Amsterdam, The Netherlands, 2022. [[CrossRef](#)]
59. Alsadaie, S.M.; Mujtaba, I.M. Dynamic modelling of Heat Exchanger fouling in multistage flash (MSF) desalination. *Desalination* **2017**, *409*, 47–65. [[CrossRef](#)]
60. Hamed, O.A. Scale control in multistage flash (MSF) desalination plants—Lessons learnt. *Desalination Water Treat.* **2017**, *81*, 19–25. [[CrossRef](#)]
61. Al-Rawajfeh, A.E.; Glade, H.; Ulrich, J. Scaling in multiple-effect distillers: The role of CO<sub>2</sub> release. *Desalination* **2005**, *182*, 209–219. [[CrossRef](#)]
62. Bourouni, K.; Martin, R.; Tadrist, L. Modelling of heat and mass transfer in a horizontal-tube falling-film evaporator for water desalination. *Desalination* **1998**, *116*, 165–183. [[CrossRef](#)]
63. Al-Rawajfeh, A.E.; Glade, H.; Ulrich, J. CO<sub>2</sub> release in multiple-effect distillers controlled by mass transfer with chemical reaction. *Desalination* **2003**, *156*, 109–123. [[CrossRef](#)]
64. Millero, F.J. Thermodynamics of the carbon dioxide system in the oceans. *Geochim. Cosmochim. Acta* **1995**, *59*, 661–677. [[CrossRef](#)]
65. Dooly, R.; Glater, J. Alkaline scale formation in boiling sea water brines. *Desalination* **1972**, *11*, 1–16. [[CrossRef](#)]
66. Langelier, W.F.; Caldwell, D.H.; Lawrence, W.B.; Spaulding, C.H. Scale Control in Sea Water Distillation Equipment—Contact Stabilization. *Ind. Eng. Chem.* **1950**, *42*, 126–130. [[CrossRef](#)]
67. Freyer, D.; Voigt, W. Crystallization and Phase Stability of CaSO<sub>4</sub> and CaSO<sub>4</sub>—Based Salts. *Mon. Fur Chem.* **2003**, *134*, 693–719. [[CrossRef](#)]
68. Watson Desalination Consultants. *Watson Desalination Consultants, Technology Review and Handbook: High Temperature Scale Inhibitors for Seawater Distillation, A Multi-Client Study*; Barnett: St. Manassas, VA, USA, 1979.
69. El Din, A.S.; Mohammed, R.A. On the thermal stability of the HCO<sub>3</sub><sup>-</sup> and the CO<sub>3</sub><sup>2-</sup> ions in aqueous solutions. *Desalination* **1988**, *69*, 241–249. [[CrossRef](#)]
70. Hasson, D.; Perl, I. Scale deposition in a laminar falling-film system. *Desalination* **1981**, *37*, 279–292. [[CrossRef](#)]
71. Al-Rawajfeh, A.E. Simultaneous desorption–crystallization of CO<sub>2</sub>–CaCO<sub>3</sub> in multi-stage flash (MSF) distillers. *Chem. Eng. Process.—Process. Intensif.* **2008**, *47*, 2262–2269. [[CrossRef](#)]
72. Al-Rawajfeh, A.E.; Glade, H.; Qiblawey, H.M.; Ulrich, J. Simulation of CO<sub>2</sub> release in multiple-effect distillers. *Desalination* **2004**, *166*, 41–52. [[CrossRef](#)]
73. Al-Rawajfeh, A.E. Influence of Seawater Composition on CO<sub>2</sub> Release and Scaling in Multi-Stage Flash (MSF) Distillers from Different Arabian Gulf Intakes. *Int. J. Chem. Eng. Appl.* **2010**, *1*, 43–48. [[CrossRef](#)]
74. Kazi, N.S. Fouling and Fouling Mitigation on Heat Exchanger Surfaces. In *Heat Exchangers—Basics Design Applications*; InTech: London, UK, 2012. [[CrossRef](#)]
75. Al-Rawajfeh, A.E.; Fath, H.E.S.; Mabrouk, A.A. Integrated Salts Precipitation and Nano-Filtration as Pretreatment of Multistage Flash Desalination System. *Heat Transf. Eng.* **2012**, *33*, 272–279. [[CrossRef](#)]

76. Al-Rawajfeh, A.E.; Ihm, S.; Varshney, H.; Mabrouk, A.N. Scale formation model for high top brine temperature multi-stage flash (MSF) desalination plants. *Desalination* **2014**, *350*, 53–60. [CrossRef]
77. Segev, R.; Hasson, D.; Semiat, R. Rigorous modeling of the kinetics of calcium carbonate deposit formation. *AIChE J.* **2012**, *58*, 1222–1229. [CrossRef]
78. Chan, S.H.; Ghassemi, K.F. Analytical Modeling of Calcium Carbonate Deposition for Laminar Falling Films and Turbulent Flow in Annuli: Part I—Formulation and Single-Species Model. *J. Heat Transf.* **1991**, *113*, 735–740. [CrossRef]
79. Bansal, B.; Müller-Steinhagen, H. Crystallization Fouling in Plate Heat Exchangers. *J. Heat Transf.* **1993**, *115*, 584–591. [CrossRef]
80. Augustin, W.; Bohnet, M. Influence of the ratio of free hydrogen ions on crystallization fouling. *Chem. Eng. Process. Process. Intensif.* **1995**, *34*, 79–85. [CrossRef]
81. Mwaba, M.; Golriz, M.; Gu, J. A semi-empirical correlation for crystallization fouling on heat exchange surfaces. *Appl. Therm. Eng.* **2006**, *26*, 440–447. [CrossRef]
82. Hasson, D.; Sherman, H.; Biton, M. Prediction of calcium carbonate scaling rates. In Proceedings of the International Symposium Fresh Water from the Sea; 1978; Volume 6, pp. 193–199.
83. Alsadaie, S.; Mujtaba, I.M. Crystallization of calcium carbonate and magnesium hydroxide in the heat exchangers of once-through Multistage Flash (MSF-OT) desalination process. *Comput. Chem. Eng.* **2018**, *122*, 293–305. [CrossRef]
84. Harris, A.; Finan, M.; Elliot, M. A theory of the formation of magnesium scales in sea water distillation plants, and means for their prevention. *Desalination* **1974**, *14*, 325–340. [CrossRef]
85. Sung-Tsuen, L.; Nancollas, G.H. The crystallization of magnesium hydroxide. *Desalination* **1973**, *12*, 75–84. [CrossRef]
86. Ciba-Geigy. *Non-Condensable Gases and the Venting of Seawater Evaporators*, Bulletin DB 2.2; Ciba-Geigy: Basel, Switzerland, 1978.
87. Ludwig, H.; Hetschel, M. Treatment of distillates and permeates from seawater desalination plants. *Desalination* **1986**, *58*, 135–154. [CrossRef]
88. Qasim, M.; Badrelzaman, M.; Darwish, N.N.; Darwish, N.A.; Hilal, N. Reverse osmosis desalination: A state-of-the-art review. *Desalination* **2019**, *459*, 59–104. [CrossRef]
89. Singh, Y.; Shahzad, M.; Ng, K. Scale formation in thermally-driven seawater desalination: Evaluation of tetrapolymer antiscalant at higher temperature operation. In Proceedings of the Twentieth International Water Technology Conference (IWTC20), Hurghada, Egypt, 18–20 May 2017.
90. De Carvalho, C.B.; Carvalho, E.P.; Ravagnani, M.A.S.S. Dynamic Analysis of Fouling Buildup in Heat Exchangers Designed According to TEMA Standards. *Ind. Eng. Chem. Res.* **2018**, *57*, 3753–3764. [CrossRef]
91. Ebert, W.; Panchal, C.B. Analysis of Exxon Crude-Oil-Slip Stream Coking Data. USDOE Assistant Secretary for Energy Efficiency and Renewable Energy. 1995; pp. 18–23. Available online: <https://www.osti.gov/servlets/purl/453433> (accessed on 14 December 2020).
92. Wang, Y.; Yuan, Z.; Liang, Y.; Xie, Y.; Chen, X.; Li, X. A review of experimental measurement and prediction models of crude oil fouling rate in crude refinery preheat trains. *Asia-Pacific J. Chem. Eng.* **2015**, *10*, 607–625. [CrossRef]
93. Polley, G.; Wilson, D.; Yeap, B.; Pugh, S. Evaluation of laboratory crude oil threshold fouling data for application to refinery pre-heat trains. *Appl. Therm. Eng.* **2002**, *22*, 777–788. [CrossRef]
94. Nasr, M.R.J.; Givi, M.M. Modeling of crude oil fouling in preheat exchangers of refinery distillation units. *Appl. Therm. Eng.* **2006**, *26*, 1572–1577. [CrossRef]
95. Shetty, N.; Deshannavar, U.B.; Marappagounder, R.; Pendyala, R. Improved threshold fouling models for crude oils. *Energy* **2016**, *111*, 453–467. [CrossRef]
96. Costa, A.L.H.; Tavares, V.B.G.; Borges, J.L.; Queiroz, E.M.; Pessoa, F.L.P.; Liporace, F.D.S.; de Oliveira, S.G. Parameter Estimation of Fouling Models in Crude Preheat Trains. *Heat Transf. Eng.* **2013**, *34*, 683–691. [CrossRef]
97. Markowski, M.; Trafczynski, M.; Urbaniec, K. Validation of the method for determination of the thermal resistance of fouling in shell and tube heat exchangers. *Energy Convers. Manag.* **2013**, *76*, 307–313. [CrossRef]
98. Jonsson, G.R.; Lalot, S.; Palsson, O.P.; Desmet, B. Use of extended Kalman filtering in detecting fouling in heat exchangers. *Int. J. Heat Mass Transf.* **2007**, *50*, 2643–2655. [CrossRef]
99. Delrot, S.; Busawon, K.; Djemaï, M.; Delmotte, F.; Dambrine, M. Fouling detection in heat exchangers. *IFAC Proc. Vol.* **2011**, *44*, 13368–13373. [CrossRef]
100. Sivathanu, A.K.; Subramanian, S. Extended Kalman filter for fouling detection in thermal power plant reheater. *Control. Eng. Pract.* **2018**, *73*, 91–99. [CrossRef]
101. Delrot, S.; Guerra, T.M.; Dambrine, M.; Delmotte, F. Fouling detection in a heat exchanger by observer of Takagi–Sugeno type for systems with unknown polynomial inputs. *Eng. Appl. Artif. Intell.* **2012**, *25*, 1558–1566. [CrossRef]
102. Lendek, Z.; Guerra, T.M.; Babuška, R.; De Schutter, B. *Stability Analysis and Nonlinear Observer Design Using Takagi–Sugeno Fuzzy Models*; Springer: Berlin/Heidelberg, Germany, 2011. [CrossRef]
103. Sun, L.; Saqi, R.; Xie, H. Research on the Fouling Prediction of Heat Exchanger Based on Wavelet Relevance Vector Machine. *Adv. Neural Netw. Res. Appl.* **2010**, *67*, 37–45. [CrossRef]
104. Dragan, D. Fault Detection of an Industrial Heat-Exchanger: A Model-Based Approach. *Stroj. Vestnik J. Mech. Eng.* **2011**, *57*, 477–484. [CrossRef]
105. Gudmundsson, O. Detection of Fouling in Heat Exchangers Using Model Comparison. Ph.D. Thesis, University of Iceland, Reykjavik, Iceland, 2015.

106. Andrjesdóttir, Ó.; Pálsson, H.; Lalot, S.; Desmet, B. Detection of fouling in a heat exchanger by application of a lock-in technique. In Proceedings of the International Conference on Heat Exchanger Fouling and Cleaning IX, Crete Island, Greece, 5–10 June 2011; pp. 373–379.
107. Lalot, S.; Desmet, B. The lock-in technique applied to heat exchangers: A semi-analytical approach and its application to fouling detection. *Appl. Therm. Eng.* **2017**, *114*, 154–162. [[CrossRef](#)]
108. Coletti, F.; Macchietto, S. A Dynamic, Distributed Model of Shell-and-Tube Heat Exchangers Undergoing Crude Oil Fouling. *Ind. Eng. Chem. Res.* **2011**, *50*, 4515–4533. [[CrossRef](#)]
109. Al Hadad, W.; Schick, V.; Maillot, D. Fouling detection in a shell and tube heat exchanger using variation of its thermal impulse responses: Methodological approach and numerical verification. *Appl. Therm. Eng.* **2019**, *155*, 612–619. [[CrossRef](#)]
110. Radhakrishnan, V.R.; Ramasamy, M.; Zabiri, H.; Do Thanh, V.; Tahir, N.M.; Mukhtar, H.; Hamdi, M.R.; Ramli, N. Heat exchanger fouling model and preventive maintenance scheduling tool. *Fuel* **2007**, *86*, 2383–2388. [[CrossRef](#)]
111. Davoudi, E.; Vaferi, B. Applying artificial neural networks for systematic estimation of degree of fouling in heat exchangers. *Chem. Eng. Res. Des.* **2018**, *130*, 138–153. [[CrossRef](#)]
112. An, Y.; Sun, X.; Ren, B.; Li, H.; Zhang, M. A data-driven method for IGBT open-circuit fault diagnosis for the modular multilevel converter based on a modified Elman neural network. *Energy Rep.* **2022**, *8*, 80–88. [[CrossRef](#)]
113. Aminian, J.; Shahhosseini, S. Neuro-based formulation to predict fouling threshold in crude preheaters. *Int. Commun. Heat Mass Transf.* **2009**, *36*, 525–531. [[CrossRef](#)]
114. Al-Naser, M.; Al-Toum, M.; El-Ferik, S.; Ben Mansour, R. Heat exchanger fouling prediction using artificial intelligence. In Proceedings of the 5th International Conference on Advances in Mechanical Engineering, Istanbul, Turkey, 17–19 December 2019; pp. 17–19.
115. Al-Naser, M.; El-Ferik, S.; Ben Mansour, R.; AlShammari, H.Y.; AlAmoudi, A. Intelligent Prediction Approach of Fouling Location in Shell and Tube Heat Exchanger. In Proceedings of the 2020 IEEE 10th International Conference on System Engineering and Technology (ICSET), Shah Alam, Malaysia, 9 November 2020; pp. 139–144. [[CrossRef](#)]
116. Schlüter, F.; Schnöing, L.; Zettler, H.; Augustin, W.; Scholl, S. Measuring Local Crystallization Fouling in a Double-Pipe Heat Exchanger. *Heat Transf. Eng.* **2020**, *41*, 149–159. [[CrossRef](#)]
117. Grosfils, V.; Kinnaert, M.; Bogaerts, P.; Hanus, R. Fouling monitoring in a thermosiphon reboiler. In Proceedings of the 2001 European Control Conference (ECC), Porto, Portugal, 4–7 September 2001. [[CrossRef](#)]
118. Yamashita, Y. Model-based monitoring of fouling in a heat exchanger. In Proceedings of the 2017 6th International Symposium on Advanced Control of Industrial Processes (AdCONIP), Taipei, Taiwan, 28–31 May 2017; pp. 453–456. [[CrossRef](#)]
119. Kuwahara, T.; Wibowo, C.; Kuboyama, A.; Nakamura, M.; Yamane, Y. Fouling Monitoring in Thermosiphon Reboiler. *Heat Transf. Eng.* **2015**, *36*, 780–786. [[CrossRef](#)]
120. Levina, T.M.; A Kireeva, N.; A Zharinov, Y.; Krasnov, A.N. Minimizing Deposit Formation in Industrial Fluid Heat Exchangers. *IOP Conf. Series: Earth Environ. Sci.* **2021**, *666*, 032007. [[CrossRef](#)]
121. White Paper. Asset Management of Mechanical Plant Components with SIMATIC PCS 7 White Paper 2013. Available online: [https://cache.industry.siemens.com/dl/files/825/109772825/att\\_1002077/v1/WhitepaperMechanicalAssets\\_EN\\_2014.pdf](https://cache.industry.siemens.com/dl/files/825/109772825/att_1002077/v1/WhitepaperMechanicalAssets_EN_2014.pdf) (accessed on 11 December 2022).
122. Real-Time Condition Monitoring for Heat Exchangers with IIoT | Yokogawa Europe. Available online: <https://www.yokogawa.com/eu/library/resources/application-notes/real-time-condition-monitoring-for-heat-exchangers-with-iiot/> (accessed on 12 November 2022).
123. Yokogawa Vigilant Plant Services: Using Applied Industry Knowledge to Solve Key End User Issues | Yokogawa Electric Corporation. Available online: <https://www.yokogawa.com/library/resources/white-papers/yokogawa-vigilantplantservices-using-applied-industry-knowledge-to-solve-key-end-user-issues/> (accessed on 12 November 2022).
124. A Two Stage Approach to Controlling Fouling on Preheat Trains at OMV's Schwechat Refinery. Available online: <https://www.digitalrefining.com/article/1001293/a-two-stage-approach-to-controlling-fouling-on-preheat-trains-at-omvs-schwechat-refinery#.Y2-153ZBxjQ> (accessed on 12 November 2022).
125. Emerson Introduces Heat Exchanger Monitoring Solution. Available online: <https://www.automation.com/en-us/products/product10/emerson-introduces-heat-exchanger-monitoring-solut> (accessed on 12 November 2022).
126. Plantweb Performance Advisor: Gas & Steam Turbine. Available online: <https://www.laurentide.com/en-ca/products/reliability/plantweb-digital-ecosystem/health-monitoring/plantweb-performance-advisor-gas-steam-turbine/> (accessed on 13 November 2022).
127. ABB. ABB Solutions for Asset Management ABB has Multiple Solutions for All Your A. Available online: [https://library.e.abb.com/public/2084cfc00ce37ed3c1257b0c00551bf9/Broch-D-AssetManagementSolutions\\_3BUS094559\\_H.pdf](https://library.e.abb.com/public/2084cfc00ce37ed3c1257b0c00551bf9/Broch-D-AssetManagementSolutions_3BUS094559_H.pdf) (accessed on 11 December 2022).
128. Phil Millette. Uniformance® Asset Sentinel for Intelligent Process Surveillance and Smarter Equipment Monitoring. In Proceedings of the 2015 Honeywell Users Gr Eur Middle East Africa; pp. 1–45. Available online: <https://pdfs.semanticscholar.org/00d3/a19c1d1bd57d71c7719430dab6eb804595eb.pdf> (accessed on 12 November 2020).
129. Asset Performance Management Apps for Industry: Using the Digital Twin to Power Predictive Analytics. Available online: <https://www.ge.com/digital/applications/asset-performance-management> (accessed on 12 November 2020).

130. GE Adds Edge Analytics, AI Capabilities to Predix Industrial IoT Suite | Computerworld. Available online: <https://www.computerworld.com/article/3234680/ge-adds-edge-analytics-ai-capabilities-to-predix-industrial-iot-suite.html> (accessed on 13 November 2022).
131. AVEVA—Global Leader in Industrial Software. Available online: <https://www.aveva.com/> (accessed on 14 November 2022).

**Disclaimer/Publisher’s Note:** The statements, opinions and data contained in all publications are solely those of the individual author(s) and contributor(s) and not of MDPI and/or the editor(s). MDPI and/or the editor(s) disclaim responsibility for any injury to people or property resulting from any ideas, methods, instructions or products referred to in the content.